IOP Publishing Journal of Physics D: Applied Physics

J. Phys. D: Appl. Phys. **56** (2023) 065401 (19pp) https://doi.org/10.1088/1361-6463/acb0dd

Towards understanding the triggering of the malignant cell death in high-efficiency magneto-mechanical anticancer therapy

P N Semina[1], I L Isaev[2], S V Komogortsev[3,5], A B Klyuchantsev[3], A S Kostyukov[1], A V Blagodatova[4], D E Khrennikov[1], A S Kichkailo[4,5], T N Zamay[4,5], I N Lapin[7], A E Sokolov[3,5,6], S P Polyutov[1,8,*] and S V Karpov[1,3,*]

[1] International Research Center of Spectroscopy and Quantum Chemistry—IRC SQC, Siberian Federal University, Krasnoyarsk 660041, Russia
[2] Institute of Computational Modelling of the Siberian Branch of the Russian Academy of Sciences, Krasnoyarsk 660036, Russia
[3] L. V. Kirensky Institute of Physics, Federal Research Center KSC the Siberian Branch of the Russian Academy of Sciences, Krasnoyarsk 660036, Russia
[4] Prof. V.F. Voino-Yasenetsky Krasnoyarsk State Medical University, Krasnoyarsk 660022, Russia
[5] Federal Research Center "Krasnoyarsk Science Center" of the Siberian Branch of the Russian Academy of Sciences, Krasnoyarsk 660036, Russia
[6] Siberian Federal University, Krasnoyarsk 660041, Russia
[7] Tomsk State University, Tomsk 634050, Russia
[8] Federal Siberian Research Clinical Center, Federal Medical Biological Agency of Russian Federation, Krasnoyarsk 660037, Russia

E-mail: spolyutov@sfu-kras.ru and karpov@iph.krasn.ru

Received 26 October 2022, revised 18 December 2022
Accepted for publication 6 January 2023
Published 23 January 2023

Abstract

The paper discusses schemes for implementing magneto-mechanical anticancer therapy and the most probable scenarios of damaging mechanical effects on the membranes of malignant cells by targeted magnetic nanoparticles (MNPs) selectively bound to membrane mechanoreceptors employing aptamers. The conditions for the selective triggering of the malignant cell apoptosis in a low-frequency non-heating alternating magnetic field, corresponding to the exceeding threshold value of the force acting on the membrane and its mechanoreceptors, are established using a nanoparticle dynamic simulation. The requirements for the functionality of MNPs and their suitability for biomedical applications are analyzed. Attention is paid to the possibility of the formation of magnetite nanoparticle aggregates in an external magnetic field and their localization near tumor cell membranes. It is shown that the scenario involving the process of aggregation of magnetite nanoparticles provides a sufficient magneto-mechanical impact to achieve a therapeutic effect. A possible explanation for the experimentally established fact of successful application of magneto-mechanical therapy using magnetite nanoparticles is presented, in which complete suppression of the Ehrlich carcinoma in an alternating magnetic field as a response to a magneto-mechanical stimulus was demonstrated. This result confirmed the possibility of using the method for high efficiency treatment of malignant neoplasms. The paper provides an extensive review of key publications and the state of the art in this area.

* Authors to whom any correspondence should be addressed.

Keywords: magnetic nanoparticle, malignant cell membrane, apoptosis, anticancer therapy, aptamer

(Some figures may appear in colour only in the online journal)

1. Introduction

1.1. Theranostics with functionalized magnetic nanoparticles

Nanotheranostics is one of the most promising and rapidly developing strategies of modern biomedicine, which implies a complex of noninvasive diagnostic and therapeutic methods combined in a single consistent and simultaneous process within a common technological platform. By now, nanotheranostics is understood to be a complex of physical principles of nanotechnological techniques, biochemical and engineering means of controlling various nanoparticles, functioning both for the intended tasks and for specific molecular targets [1–6].

Nanotheranostics aimes to eliminate many fundamental drawbacks of traditional methods of diagnosis, treatment, and monitoring, in which widely used means of modern medicine and the effect of injected drugs are not targeted, in particular in the treatment of oncological diseases. They are spread throughout the organism by the bloodstream and therefore have to be injected in unnecessarily large quantities compared to the doses actually needed to treat the affected tissue, which can often exceed the toxicity limit and become below the therapeutic threshold after some time.

Among nanotheranostic approaches using various physical principles, noninvasive control of the biochemical system through non-heating low-frequency electromagnetic fields should be noted. Exposure of the organism to low-frequency electromagnetic fields poses far fewer risks and dangers than chemical and radiation exposures, let alone surgical ones. At the same time, low-frequency electromagnetic fields themselves are easy to dose and control, and the impact on the affected organ can be focused in any area of the internal organs with a size of about a few millimeters.

When choosing the frequency of the electromagnetic field, it should be considered that the depth of field penetration increases as its frequency reduces. Alternating magnetic fields that cause negligible heat release and temperature change compared to metabolic heat generation can be considered non-heating. Low-frequency magnetic fields with a frequency of much less than 1000 Hz are guaranteed to be non-heating under any conditions with or without the use of magnetic nanoparticles (MNPs) [7].

The main disadvantage of nanoparticles, until recently, was the non-selectivity of their bonding, which occurs not only with diseased but also with normal tissues, accompanied by the negative impact in the alternating magnetic field [8, 9]. This drawback has been overcome by targeting delivery with recognition agents that specifically bind to cancer cell biomolecules.

Among the most promising recognition agents are aptamers, short synthetic single-domain DNAs that specifically bind to various targets such as organic molecules, proteins, cells, and tissues with high binding selectivity [10–12]. Their low toxicity and cost are also noteworthy.

Thus, methods of targeted exposure to the malignant cells are the basis of the strategy of anticancer therapy using various physical factors.

Magnetic nanotheranostics, which, along with diagnostics, also includes the treatment of malignant neoplasms using targeted MNPs [7, 13–20], has several advantages over laser photodynamic therapy methods e.g. [21–24], as well as chemical e.g. [24], hydrodynamic [25–29] and radiation effects on the organism. The laser radiation intensity must be controlled to prevent intense heating of the nanoparticles accompanied by a loss of their resonance properties [30–32].

The prevalence of MNPs is extensively increasing, and their applications are very diverse. Superparamagnetic nanoparticles are the most popular since they exhibit magnetic properties only when a magnetic field is applied. The magnetic moment of superparamagnetic nanoparticles without a magnetic field is zero [33, 34]. Note that this feature prevents fast spontaneous aggregation of superparamagnetic nanoparticles.

The use of MNPs for therapy is possible when the magnetic core is modified with: (a) a biologically functional layer providing interaction with the target; (b) a protective shell that ensures MNPs' stability in the organism and protects the body from the toxic effects of the magnetic core [35].

Low-frequency magnetic fields do not cause non-selective cellular hyperthermia. The therapeutic effect due to the mechanical impact on the cell membrane is associated with less damaging factors for normal cells. The high penetrating ability of the alternating magnetic field provides treatment efficacy and versatility of application to various types of malignant neoplasms.

Magnetic nanotheranostics with functionalized single-domain MNPs using alternating magnetic fields as well as drug delivery applications are reviewed e.g. in papers by Golovin *et al* [7, 14, 36]. The papers mainly focus on a new approach that utilizes non-heating low frequency magnetic fields for the nanomechanical actuation of MNPs.

An important aspect of this method is the ability to control the dose and exposure time of the therapeutic effect.

The problem of the active targeted delivery of MNPs to a pathological molecule for cancer diagnostics and therapy is one of the most acute problems. It can be solved by creating nanostructures conjugated with molecular recognition ligands. Nucleic acid aptamers can easily match any desired target due to their ability to form unique conformation. This small artificial single-stranded RNA or DNA oligonucleotide can be designed to bind with high affinity and specificity to any molecule or cell. Through structural recognition, aptamers recognize and bind specifically to given cells *in vivo* [37–39].

In addition, aptamers are produced chemically and chemically modified in an easily scalable process; the synthesis is not susceptible to viral or bacterial contamination. Oligonucleotides are non-immunogenic and non-toxic, small size allows them to penetrate any tumors. They reversibly denature with the restoration of the desired conformation. An significant advantage is that the production of aptamers is approximately 100 times cheaper than monoclonal antibodies [40].

Another problem with using MNPs for cancer therapy is their high reactivity, efficient diffusion through biological membranes, and ability to overcome tissue barriers, which increase their toxicity to normal tissues [41].

Moreover, MNPs toxicity is determined by their chemical composition. It is assumed that MNPs based on iron are less toxic since iron is quickly degraded in the body. Manganese (Mn) and zinc (Zn) are more toxic than iron and are practically not used without prior surface modification [42].

The following types of MNPs are known for application in magneto-theranostics e.g. $FeCo, FePt, CoPt, Co, Ni, CoFeO_4$, Fe_2O_3, Fe_3O_4 [7]. Note the moderate biocompatibility of magnetite Fe_3O_4, which is its important advantage. MNPs consisting of this material will be the subject of our work.

Note that Co and Ni used for magnetic hyperthermia are highly toxic and require special coatings [43]. However, the functionalization of MNPs with aptamers reduces toxicity and increases the biocompatibility of MNPs [35].

A striking example of the successful realization of a high-efficiency magneto-mechanical therapy using MNPs functionalized with aptamer, providing targeted delivery of MNPs to the mouse Ehrlich carcinoma cells *in vivo* and *in vitro* is the paper by Belyanina *et al* [13]. In this work, aptamer AS-14 selectively stuck MNPs with the extracellular matrix fibronectin. It was shown that 10 min exposure to an alternating magnetic field with a frequency of 50 Hz caused tumor cell apoptosis (programmed cell death) without heating. These studies confirmed the possibility of using MNPs functionalized by aptamers in an alternating non-heating magnetic field for the successful therapy of malignant neoplasms.

The range of applications of MNPs for biomedical applications is quite broad. They can be used for targeted drug delivery [44–47]. One of the first communications on the targeted delivery of the anti-tumor medication epirubicin *in vivo* as part of a ferrofluid with MNP to which it was chemically bound was made in paper [48]. In addition, MNPs can be used to enhance the contrast of magnetic resonance imaging [46, 49, 50], for diagnosis [51, 52], detecting molecules when nanoparticles bind to them [53, 54], imaging [55], bioseparation [56–59], and as a component of biomaterial for tissue engineering [60], etc. In addition, the use of MNPs (Janus nanoparticles in paper [61]) allows the creation of a strategy to stimulate the body's T-lymphocytes to produce a natural immune response, which is an important step in immunotherapeutic protocols.

In theranostics of malignancies [34, 62] based on the application of MNPs, the choice of their characteristics, such as saturation magnetization and magneto-crystalline anisotropy, which depends on the chemical composition of nanoparticles and their shape, corresponding to a specific therapeutic task [63, 64]. The interrelation of these parameters optimizes the magnetic characteristics for effective theranostics. The review [65] considers cellular effects (primarily the death of the malignant cells or pathogens) that depend on the combination of the above parameters and are determined by the composition and size of MNP, the exposure time of the magnetic field, its frequency and intensity. Functionalization of the nanoparticle surface, in addition to the ability to recognize the malignant cells, also allows solving the problem of biocompatibility [35, 66]. The choice of material, composition, size of MNPs, and method of functionalization of their surface is dictated by the following requirements: low toxicity of the obtained bioconjugate, the single-domain structure of MNPs for uniform magnetization in an external magnetic field, localization of the magnetic field within the exposure area, and the possibility immobilizing molecules on the MNP surface for targeted delivery [35, 67].

Synthetic oligonucleotides, single-stranded DNA aptamers [68, 69] are one of the essential bioconjugate components that provide selective interaction with the tumor cells. Aptamers are of great interest for interdisciplinary research in molecular biology and physics because they can be easily immobilized onto various carriers, such as nanoparticles of various shapes and sizes. DNA or RNA oligonucleotides have a high affinity and specificity to the target [38, 70]. The targets of aptamers can be either whole cells or individual molecules. Aptamers of different sizes are obtained by the systematic evolution of ligands by exponential enrichment [71] selection from a sequence library.

1.2. Scenarios of the malignant cell apoptosis and related processes involving the cell membrane elements

It should be noted that the initiation of apoptosis is not due solely to the mechanical effect on the mechanoreceptors of the malignant cell membrane using MNPs. Such exposure only triggers a cascade of accompanying biochemical processes with the involvement of cell elements implicated in the initiation of apoptosis [72]. Some of the most important biochemical processes are worth discussing here.

The selective binding of DNA aptamer to the malignant cell is due to its affinity for fibronectin, as well as its affinity for integrin, a receptor transmembrane protein [73]. Functionally, integrin connects the cell's internal environment with the external environment—the extracellular matrix, including through fibronectin [74, 75].

Fibronectin stimulates signal transduction and participates in cell cycle evolution [76–78] by being linked to integrin.

A key role of integrin for the cell is its signaling function, providing various scenarios of intracellular reactions in response to external influences [79–82], including apoptosis. The binding of fibronectin to integrin is accompanied by a change in the conformational state of the latter [83, 84].

Apoptosis can be triggered externally by specific transmembrane proteins—death receptors [85–87]. In addition, the formation of the apoptotic signal can be initiated by the binding of NPs to proteins that play a key role in tumor growth [88]. For example, superparamagnetic nanoparticles (NiFe and magnetite nanodisks) used in [89] and functionalized for binding to the renal carcinoma tumor membrane antigen (CA9 [90] carboanthidase) induced apoptosis 6 h after bioconjugate injection and exposure to a non-heating (≈30 mT) low-frequency (≈20 Hz) magnetic field.

As a result, the proteins that block apoptosis lose activity, and the cytoskeleton and nuclear membrane are destroyed. The cell disintegrates into apoptotic corpuscles with their subsequent capture by immune system cells and phagocytosis [91].

Note that apoptosis is accompanied by the formation of macromolecular complexes in which the activation of enzymes—caspases occurs, which serves as a signal for the initiation of a cell death program [92–94]. Caspases trigger cell death by cleaving specific proteins in the cytoplasm and nucleus.

Importantly, caspases are experimental markers for the registration of apoptosis and their presence is indicative of the initiation, and course of this process in the malignant neoplasms [18, 89, 95, 96]. For example, the interaction of Fas Ligand (FasL) and Tumor Necrosis Factor Ligand Superfamily, Member 10 (TNFSF10) with receptors initiate the apoptotic processes, which is accompanied by the formation of a death-inducing signaling complex that activates caspase-8 [91, 97].

Specific binding of the bioconjugate to the malignant cell under alternating magnetic field conditions, which does not result in a hyperthermic effect, ensures that intracellular scenarios trigger apoptosis[81, 82] as follows: aptamer-bound fibronectin, when coupled to integrin, causes its conformation to change [83, 84, 98, 99], and the presence of MNP in the extracellular matrix under the alternating magnetic field causes a mechanical pulling effect on integrin.

According to the approach [13, 83, 98, 100, 101] used in our work, the mechanical action on transmembrane proteins (including integrin) changes their conformation, taking into account the contribution of ligand binding, can initiate cellular reactions.

Importantly, triggering of the caspase cascade by mechanical action on integrin using MNPs in an alternating magnetic field in work [13] is evidence of apoptosis in the Ehrlich carcinoma cells. To effectively trigger apoptosis, it is important to know the threshold magnitude of the force that must be applied to the transmembrane protein to accelerate its conformational transition. The magnitude of this force, which causes cell death, ranges from 4 pN [100, 101] to 10 pN. The maximum value corresponds to the threshold value of the force at which the bond between the integrin and the ligand can be broken and through which the mechanical pulling action is transmitted [102].

Mechanical activation of select signaling pathways may be combined with other (systemic) stimuli to induce cell death. In [100, 101] it has recently been demonstrated that the activation of extracellular signal-regulated kinase pathway through periodic stretching specifically targeted ErbB3 receptors in MCF7 cells with 4 pN using micrometer-long iron rods with functionalized gold tips.

Cell adhesion (association) processes play an important role in the development of apoptosis [103]. If, for some reason, the cell lacks signaling interactions with the intercellular matrix, the cell cycle ceases, and the caspase cascade is activated, leading to apoptosis [104] is initiated.

In the literature, mechanisms for triggering apoptosis, where integrins play an essential role, have been described in [84, 105–108]. One of them is anoikis, a type of cell death associated with cell detachment from neighboring cells [109] with the sequence of biochemical processes in the cell leading to apoptosis [91, 109]. The second variant is integrin-mediated apoptosis, which occurs due to the disruption of integrin-ligand contact [98]. Ligand-unbound integrins can lead to subsequent activation of caspase-8 [104].

The goals of our paper are: (a) investigation of the conditions in which the mechanical motion of an MNP bound explicitly to a malignant cell by a DNA aptamer can create a force applied to a transmembrane protein under the action of an alternating magnetic field exceeding the threshold required to trigger apoptosis through the formation of an intracellular signaling pathway; (b) an explanation of the experimental result [13], which demonstrated effective suppression of the Ehrlich carcinoma cell division using magnetite particles in an alternating magnetic field as a response to a magneto-mechanical stimulus.

The paper is organized as follows. In section 1, a literature review of the topic of the study and related issues are given, as well as the goals of the study are formulated. Section 2 describes the models of the nanoparticle motion in an alternating magnetic field, ensuring the exceeding of the threshold force on the transmembrane protein, as well as the physical and structural properties of nanoparticles and the schemes of their interaction with each other and with the cell membrane. Section 3 describes the nanomaterials used in the experiments. Section 4 presents the kinetics of the interaction of nanoparticles with the membrane in an alternating magnetic field, the dependencies of the exposure force on the size of MNPs and the magnetic field strength, as well as the aggregation effect of MNPs and its influence on the impact force on the cell mechanoreceptors.

2. Model of mechanical interaction of MNPs with a cell membrane

The application of various physical factors of targeted exposure to malignant cells is one of the important areas of research when determining the strategy for anticancer therapy.

In our work, we consider a model simulating the conditions of an actual experiment [13] using MNPs ('core–shell' nanoparticles covering size ranges 30–50 nm with a magnetite core of 11–15 nm diameter and the Au shell) with AS-14 DNA aptamers conjugated on its surface, as well as magnetite nanoparticles of heterogeneous hydrosols consisting of individual gold and magnetite nanoparticles. The aptamers on the gold surface of MNP recognize a specific fibronectin domain and provide a binding site, while the other fibronectin domain interacts with the binding site located on the β-subunit of integrin [73, 83, 98].

Thus, the selectivity of aptamer binding to malignant tumor cells through the transmembrane protein—integrin and its ligand is realized.

In the actual experiment, the specificity of the DNA aptamer with the target is provided by a unique set of amino acid sequences, which in this case, distinguishes the fibronectin of a normal cell from the fibronectin of a malignant cell and forms the selectivity of the aptamer bond only with the latter [75, 77, 110, 111].

To reduce the cytotoxicity of MNP [112–115], as well as to realize the binding of the bioconjugate to the target, their combination with gold nanoparticles in the studied hydrosol or 'core–shell' nanoparticles (gold shell and magnetite core) [54, 116] is used. In addition, conjugation with DNA-aptamers can be performed by decorating magnetite nanoparticles with gold fragments on the particle surface.

The cause of the force effect on cell mechanoreceptors is the motion of MNP in an alternating magnetic field. Such a motion of MNP bound to the membrane is caused by the rotational component of this movement emerged by the tendency to align the intrinsic magnetic dipole moment of MNPs along the direction of the applied magnetic field. In the free state, such particles rotate around their axis, and when the field direction is reversed, the rotation changes to the opposite until the magnetic moment is aligned along the field.

In a simplified case of MNP binding to a membrane in its specific area, limited by the size of the aptamer (within 10 nm [117]), as well as a fragment of fibronectin fiber and integrin, the character of particle motion is an arc, the length of which is limited by the contact condition membrane particle on the left and right, as shown in figure 1. It is also important to note that MNP deforms the membrane at the site of contact with it and, during rotation, creates a moment of force that has a vertical projection, which is applied to the transmembrane protein integrin (or to another membrane element with which a connection can selectively occur)

In addition, at the moment when the particle touches the membrane, several elements act on it: an aptamer rigidly bound to fibronectin, which, in turn, is bound to the transmembrane protein. The size of the integrin above the outer surface of the membrane in the open conformational state is about 19 nm [83].

The action of an alternating magnetic field on MNPs can be accompanied by two ways of relaxation processes of ferrimagnetic single domains: the Brownian and Neel relaxation [7]. The latter is associated with thermal fluctuations in magnetic anisotropy, leading to changes in both orientation and amplitude of the nanoparticle magnetic dipole moment.

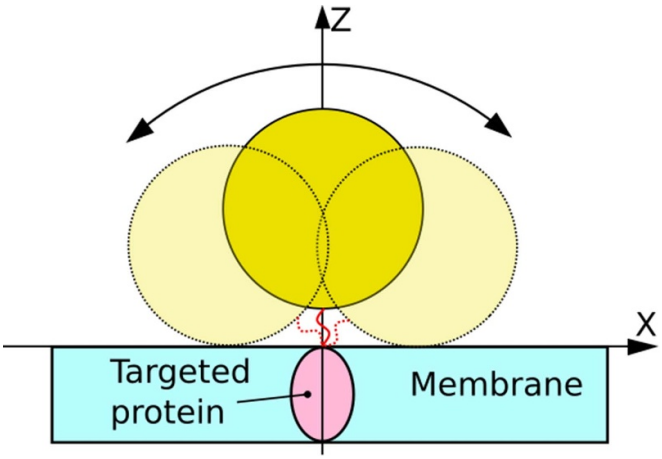

Figure 1. The schematic motion of a magnetic nanoparticle bound to a specific area of a cell membrane in an alternating magnetic field.

2.1. Equations of motion of a MNP in an alternating magnetic field

The equation of motion of a free MNP under the action of an alternating magnetic field includes the vectors of the nanoparticle's intrinsic magnetic moment **M** and magnetic field induction **B**, responsible for the particle's rotation and achievement of the orientational equilibrium condition [7]. These conditions correspond to the collinearity of the magnetic moment and field direction, taking into account the action of the rotational viscous friction torque [118, 119]

$$I\frac{\mathrm{d}^2\phi}{\mathrm{d}t^2} = -M\cdot B(t)\sin\phi - 8\pi\eta R_m^3\frac{\mathrm{d}\phi}{\mathrm{d}t}. \tag{1}$$

The motion of MNP in conditions of its bonding with the cell membrane surface through the aptamer in the alternating harmonic magnetic field is an oscillatory process corresponding to the periodic motion of the particle center of mass along an arc within a certain angle (figure 1).

Such translational-rotational dynamics of a particle (without taking into account the stochastic force [119]) obeys the following system of equations [14,118,119]

$$m\frac{\mathrm{d}^2\mathbf{r}_i}{\mathrm{d}t^2} = \mathbf{F} - 6\pi\eta\mathrm{R_m}\frac{\mathrm{d}\mathbf{r}_i}{\mathrm{d}t}, \tag{2}$$

$$I_{ij}\frac{\mathrm{d}^2\boldsymbol{\phi}}{\mathrm{d}t^2} = [\mathbf{M},\mathbf{B}] - [\mathbf{x}_0,\mathbf{F}] - 8\pi\eta\mathrm{R_m^3}\frac{\mathrm{d}\boldsymbol{\phi}}{\mathrm{d}t}. \tag{3}$$

In equations (1)–(3) $\boldsymbol{\phi}$ is the angle of the current direction of the MNP magnetic moment relative to the direction vector of the external alternating magnetic field in the first half-period, I_{ij} is the moment of inertia tensor of MNP, m is the nanoparticle mass, R_m is the hydrodynamic radius of a particle, **F** is the elasticity force acting on nanoparticle from aptamer, $\mathbf{x}_0$ is the radius-vector from the MNP center to applied force point,

η is the viscosity of the environment (accepted as the equivalent of water sim10^{-3} Pa·s). The viscosity of the intracellular fluid may significantly exceed the characteristic values for water [7].

Equation (2) also includes the force of viscous friction arising from the translational motion of a particle in a viscous medium.

2.2. *The effect of a MNP on the membrane in an alternating magnetic field*

It should be taken into account that different types of hydrosols with biocompatible nanoparticles were used in experiments on magneto-mechanical therapy, including heterogeneous hydrosols with particles of varying compositions, which included gold and magnetite nanoparticles.

First of all, we note that any combination must contain a gold particle or gold fragments on the surface of the MNP. This is due to the fact that aptamers conjugate only to gold. Thus, particles that do not contain aptamers on their surface are not able to selectively bind to the malignant cells.

Consider the most general case, in which a certain type of the MNPs under identical conditions allows the effect on an arbitrary membrane element, to which an affinity to the aptamer is created by selection. In this case, the vertical component of the force acting on the membrane and directed outward by the rotation of the particle appears figure 2.

2.2.1. Scheme of the interaction of a magnetite particle with a membrane. Considering a single magnetite particle, we assume that in synthesizing heterogeneous hydrosol (magnetite–gold), at least a small fraction of magnetite particles may contain fragments of gold on the surface. On this basis, we obtain the value of the vertical projection of the force ($\mathbf{F}_n$) acting on the membrane (figure 2(a)):

$$|\mathbf{F}_n| = \frac{\mathrm{T}}{\sqrt{2\mathrm{R}_m L}} = \frac{4\pi m_s |\mathbf{B}| \mathrm{R}_m^{5/2}}{3\mu\mu_0\sqrt{2\mathrm{L}}}, \tag{4}$$

where $\mathbf{F}_n$ is the normal projection of the elastic force acting on the aptamer, $\mathrm{T} = |\mathbf{T}| = |[\mathbf{M} \times \mathbf{H}]|$ is the maximal value of the force momentum acting on the particle, $\mathbf{H}$ is the external magnetic field strength $\mathbf{H} = \mathbf{B}/\mu\mu_0$ ($|B| = 0.01$T), μ_0 is the magnetic constant, μ is the magnetic permeability of intercellular medium (taken equal to the magnetic permeability of water), $\mathbf{M}$ is the particle's intrinsic permanent magnetic moment $|\mathbf{M}| = m_s \cdot \mathrm{V}_m$, m_s is the saturation magnetization of magnetite depending on particle size (for magnetite particles with diameter $2\mathrm{R}_m = 15$ nm $m_s = 410\,\mathrm{kA\,m^{-1}}$ [120]), $\mathrm{V}_m = (4/3) \cdot \pi \mathrm{R}_m^3$ is the volume of the magnetite particle, R_m is its radius, the magnetite density is $\rho_m = 5240\,\mathrm{kg\,m^{-3}}$ [120], $\mathrm{L} = \mathrm{L}_1 + \mathrm{L}_2 + \mathrm{L}_3$ is the length of the molecular bond (equal to the sum of the lengths of the supramembrane part of the integrin—L_1, the part of the fibronectin fiber between domains 5 and 10—L_2 that selectively connects the aptamer to the integrin, and the aptamer—L_3).

Below is the equation for the force ($\mathbf{F}_n$) acting from the dumbbell-shaped MNP, including gold and magnetite particles (figure 2(b))

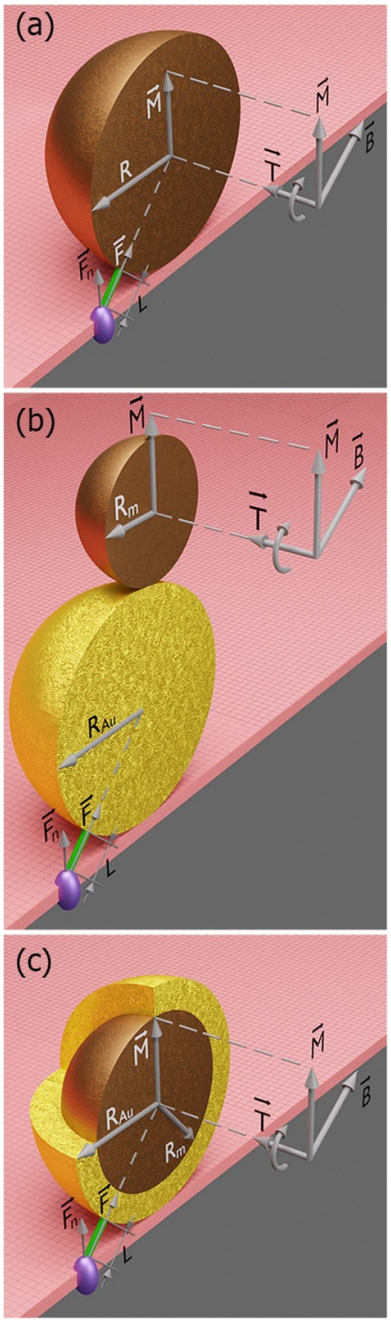

Figure 2. Schematics of three particle configurations (sectional view): (a)—single magnetite particle, (b)—magnetite particle on the surface of the gold particle (a dumbbell-shape), (c)—a particle with a magnetite core and gold shell (Blender software).

$$|\mathbf{F}_n| = \frac{4\pi m_s |\mathbf{B}| \mathrm{R}_m^{5/2}}{3\mu\mu_0\sqrt{2\mathrm{L}}} \cdot \sqrt{\frac{\mathrm{R}_m}{\mathrm{R}_{\mathrm{Au}}}}, \tag{5}$$

where R_m is the radius of MNP located on the surface of a homogeneous gold particle of radius R_{Au}.

Finally, the equation for the force ($\mathbf{F}_n$) created by the 'magnetite core–gold shell' particle is presented as follows (figure 2(c))

$$|\mathbf{F}_n| = \frac{4\pi m_s |\mathbf{B}| \mathrm{R}_m^{5/2}}{3\mu\mu_0\sqrt{2\mathrm{L}}} \cdot \frac{1}{\sqrt{1 + (\mathrm{R}_{\mathrm{Au}} - \mathrm{R}_m)/\mathrm{R}_m}}, \tag{6}$$

where R_m, R_{Au} are the radii of the magnetite core of the particle and the outer gold shell of MNP.

As can be seen from the presented equations and combinations of particles, the maximum force on the membrane is exerted by a single MNP with the same size in each of the three variants.

Figure 3(a) shows the initial position of the nanoparticle with magnetic moment (at $\mathbf{B} = 0$) and its connection to the membrane through the 'aptamer-(the fragment 5–10 fibronectin)-integrin' fragment in the absence of a magnetic field ($\mathbf{B} = 0$). Figure 3(b) shows the transition of the particle to the extreme right position after turning on the vertically directed magnetic field and the change of direction of the magnetic moment of the particle under the action of the rotational momentum ($\mathbf{T}$).

This transition occurs during the half-period of the alternating field ($t/2$), in which the field is directed vertically upward. In this new position, the particle touches the membrane at point (A), the fulcrum. Clockwise rotation of the nanoparticle is accompanied by the tension of the aptamer and the fibronectin fragment with the transfer of the pulling force to the integrin.

Because of the clockwise rotation of the particle in this scheme, a vertically directed pulling force ($\mathbf{F}_n$) acting on the integrin arises, and the arm of the force is equal to the radius of the particle. After reversing the direction of the magnetic field, the particle moves to the left of the integrins and touches the membrane.

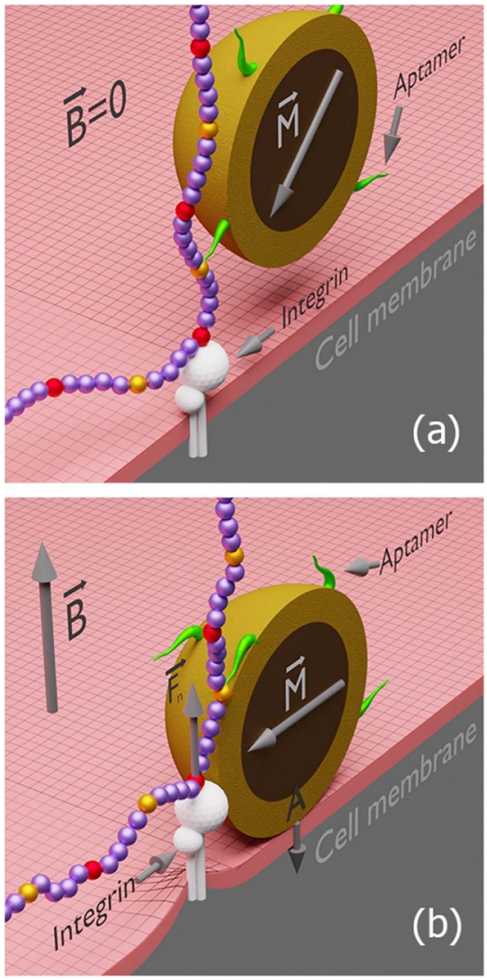

Figure 3. Schematic of the formation of the vertical projection of the pulling force ($\mathbf{F}_n$) acting on the membrane. (a)—initial position of MNP with magnetic moment ($\mathbf{M}$) and its connection with the membrane through the 'aptamer—fibronectin (its domain 5 marked in yellow and domain 10 marked in red)—integrin' sequence (in the absence of magnetic field); (b)—MNP in the extreme right position with fulcrum A after activation of the magnetic field and changing the direction of the magnetic moment of the particle ($\mathbf{M}$) (field is directed vertically). The size of the supramembrane part of the integrin is $L_1 = 19$ nm, the length of the fibronectin fragment from domain 5 to domain 10—$L_2 = 13.5$ nm, the size of the aptamer—$L_3 = 10$ nm [34]. The diameter of the 'core–shell' particle is $2R = 40$ nm, and the diameter of the magnetite core is $2R_m = 15$ nm. In the position on the right—the aptamer and fibronectin fragments 5–10 are tightly adjacent to the surface of the MNP gold shell (Blender software).

2.2.2. Scheme of a magnetite particle interaction with membrane and via exoskeleton elements. Figure 3 shows a scheme of interaction of MNP with a single fiber of fibronectin (the particle touches the membrane in extreme positions, as in figure 1), taking into account the actual size of the outer part of the transmembrane protein, integrin.

The extracellular space contains variously extended polymeric fibers as elements of the exoskeleton, among which fibronectin is worth special attention.

Figure 4 shows the scheme of interaction of MNP with two isolated fibers of fibronectin. In this scheme, MNP rotating in the alternating magnetic field does not touch the membrane, and the effect on the cell mechanoreceptors (integrin) is performed through the fibronectin fragments located in the extracellular space. This scheme is among the most realistic and takes into account the actual configuration of the exoskeleton elements. Note that there are two forces shown here: one acts on the membrane from below through the fibronectin and is directed upward, while the other force, directed downward, acts through the fibronectin on the adjacent cell located above (its membrane is shown in the figure).

The position of the nanoparticle with magnetic moment ($\mathbf{M}$) depends on its connection to fibronectin fragments. Both fibronectin fibers are connected to the membrane via integrins, and to the membrane of another cell (or an array of cells). Both fibers are connected to the aptamers, which in turn are bound to the particle surface through the fibronectin domain 5, and the lower part of the fibronectin is connected to the integrin through its domain 10. The direction of the magnetic field in this scheme is vertical, which, if the magnetic moment orientation of the particle is noncollinear, causes its counterclockwise rotation, generating the vertical component of the force ($\mathbf{F}_n$) applied to the integrin; the shoulder of the force is equal to the diameter of the particle.

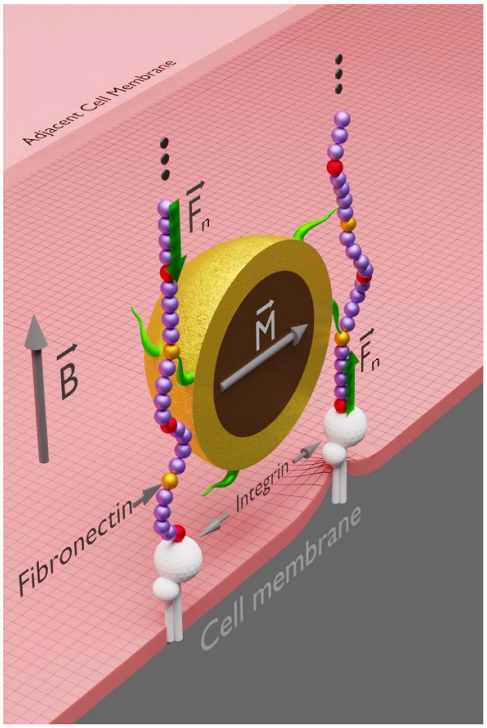

Figure 4. Schematic of the force generation ($\mathbf{F}_n$) applied to the membrane when MNP is positioned between two fibronectin fragments located in the intercellular space (three dots at the upper part of fibronectin mean its continuation towards the adjacent cell) (Blender software).

2.3. Magneto-dipole interactions of magnetite nanoparticles in the magnetic field and the formation of multiparticle aggregates in the Brownian dynamics model

It was shown above that the estimates of the value of the normal force projection according to the presented equations (4)–(6) appear below the threshold value at any variant of the geometry of magnetite particles, whose size corresponds to the actual experiment conditions, including the value of the magnetic field strength. Overcoming the problem lies in taking into account an important factor—the possibility of aggregation of MNPs with each other under the action of the magnetic field and the growth of these aggregates around the gold particle associated with the integrin, as the center of aggregation, under the action of the van der Waals attraction. The growth of multiparticle aggregates leads to an increase in their effective volume and, consequently, their total magnetic dipole moment.

As shown in [121], even plasmonic nanoparticles can aggregate during binding to the membrane. For MNPs, this possibility is discussed in the section 4.

In our work, we considered the model of interaction of a single-domain magnetite nanoparticle (Fe_3O_4), bound to the membrane of the malignant cell by a specific aptamer in a non-heating alternating magnetic field of low frequency (50 Hz).

In malignant tumor therapy, ferrimagnetic or superparamagnetic nanoparticles are used to reduce the risk of biotoxicity either in 'core–shell' form with a gold shell or in a heterogeneous hydrosol that includes biocompatible gold and magnetite nanoparticles (the latter may have an adsorption layer of polyethylene glycol, giving complete biocompatibility and additional resistance to the particle coagulation).

According to the conditions of the experiment [13], the calculations take the value of magnetic field induction $\mathbf{B} = \mu_0\mathbf{H}$ equals to 0.01 T (the field strength $\mathbf{H} = 7958\ \mathrm{A\,m^{-1}}$).

The energy of the pairwise long-range dipole–dipole interaction of permanent magnetic dipoles of magnetite particles $(U_{\mathrm{dd}})_{ij}$ in a colloidal system in the presence of magnetic field $\mathbf{B}$ corresponds to the equation

$$(U_{\mathrm{dd}})_{ij} = \frac{\mu_0}{4\pi}\left[\frac{(\mathbf{M}_i\cdot\mathbf{M}_j)r^2 - 3(\mathbf{M}_i\cdot\mathbf{r})(\mathbf{M}_j\cdot\mathbf{r})}{r^5}\right]. \tag{7}$$

The condition for calculations is the co-directionality of vectors of magnetic dipole moments of single-domain particles and the magnetic field. Accordingly, for the dipole–dipole pair interaction force, we have

$$(\mathbf{F}_{\mathrm{dd}})_{ij} = -\frac{\partial(U_{\mathrm{dd}})_{ij}}{\partial\mathbf{r}}. \tag{8}$$

The force of viscous friction $(\mathbf{F}_{\mathrm{v}})_i$ acting on NP moving at speed $\mathbf{v}_i$ is described by the Stokes law

$$(\mathbf{F}_{\mathrm{v}})_i = -6\pi\eta\,(\mathrm{R_i} + \mathrm{h_i})\,\mathbf{v}_i, \tag{9}$$

where η is the dynamic viscosity of an ambient liquid, h_i is the thickness of the nanoparticle absorption layer. In general, the dynamic viscosity $\eta = \eta(T)$ depends on the medium temperature.

The forces of tangential friction [122] occur when the particles in an aggregate shift transversely. To simplify, it can be introduced by analogy with dry friction forces (although they are not such forces). In this case, the coefficient of friction is an effective parameter that characterizes the degree of interaction of particle adsorption layers. Due to the strong intermolecular interaction of the nanoparticle adsorption layers and their unequal deformation, the effective coefficient of friction can significantly exceed one.

The direction of the tangential friction force is opposite to the projection of the velocity vector of particle's relative motion $(\mathbf{v}_j - \mathbf{v}_i)$ on the plane of their contact. Thus, the friction force acting from the *i*th nanoparticle on the *j*th particle is determined by the following equation

$$(\mathbf{F}_{\mathrm{f}})_{ij} = -\chi\left|(\mathbf{F}_{\mathrm{el}})_{ij}\right|\mathbf{q}_{ij}, \tag{10}$$

where χ is the effective coefficient of friction, $\mathbf{q}_{ij}$ is the normalized projection of the velocity of relative particles motion on the plane of the adsorption layer contact.

$$\mathbf{q}_{ij} = \frac{(\mathbf{v}_j - \mathbf{v}_i) - \mathbf{n}_{ij}\,((\mathbf{v}_j - \mathbf{v}_i)\,\mathbf{n}_{ij})}{\left|(\mathbf{v}_j - \mathbf{v}_i) - \mathbf{n}_{ij}\,((\mathbf{v}_j - \mathbf{v}_i)\,\mathbf{n}_{ij})\right|}, \tag{11}$$

where $\mathbf{n}_{ij} = \frac{\mathbf{r}_{ij}}{|\mathbf{r}_{ij}|}$ is the normalized unit vector connecting the centers of contacting particles. The total tangential friction force consists of the friction forces acting on the *i*th nan-

oparticle and determines the resistance of an nanoparticle aggregate to deformation

$$(\mathbf{F}_{\mathrm{f}})_i = \sum_{\substack{j=1 \\ i\neq j}}^{N} (\mathbf{F}_{\mathrm{f}})_{ij}. \tag{12}$$

For the hydrosols applied in the experiments, the electrostatic type of stabilization was used associated with the formation of electric double layers (EDLs) at the particle surface. The repulsion potentials of such particles are described by a screened electrostatic interaction.

For the range of small electric potentials, the total energy of interacting particles is equal to the sum of energies of the electrostatic repulsion and the van der Waals attraction. For the energy of the screened electrostatic repulsion, we have

$$U(r) = Z^2 \lambda_{\mathrm{B}} \left[\frac{\exp(\kappa \mathrm{R_i})}{1+\kappa \mathrm{R_i}}\right]^2 \frac{\exp(-\kappa r)}{r} - U_{vdw}, \tag{13}$$

where $\lambda_{\mathrm{B}} = \mathrm{e}^2/(4\pi\varepsilon\varepsilon_0 k_{\mathrm{B}}\mathrm{T})$, k_{B} is the Boltzmann constant; $\kappa^2 = 4\pi\lambda_{\mathrm{B}}\mathrm{n}$, e is the elementary charge, ε is the relative dielectric constant of the ambient medium and ε_0 is the vacuum permittivity, Z and $\mathrm{R_i}$ are the charge and radius of MNP, n is concentration of electric charges in the electrolyte.

The citrate method for the synthesis of nanoparticles with an adsorption layer thickness of up to 7.5 nm [123] is among the common ones. It should be taken into account that the salt concentration is about 150 mM [124] and, accordingly, the Debye radius is about 0.8–1 nm. Adding water to the citrate hydrosol and reduction of the electrolyte concentration does not result in the desorption of citric acid anions from gold or magnetite nanoparticles as potential-determining anions, nor in the washout of counterions from EDL. In this case, the thickness of the dense part of the particle EDL does not fall below 1 nm, which increases the resistance of magnetite particles to coagulation and slows down the rate of this process.

Note that to stabilize particles in hydrosols and to slow down aggregation [125], polymeric adsorption layers are formed on the particle surface, so the interaction between particles is fairly well described by the elastic repulsion potential of such hydrated layers upon particle collision. Such interactions are considered in more detail in the paper [126].

Here the short-range van der Waals interparticle attraction energy is described by the Hamaker–de Boer equation [122, 127]

$$(U_{\mathrm{vdw}})_{ij} = -\frac{A_{\mathrm{H}}}{6}\left(\frac{2\mathrm{R_i}\mathrm{R_j}}{\mathrm{h_{ij}^2}+2\mathrm{R_i}\mathrm{h_{ij}}+2\mathrm{R_j}\mathrm{h_{ij}}} + \frac{2\mathrm{R_i}\mathrm{R_j}}{\mathrm{h_{ij}^2}+2\mathrm{R_i}\mathrm{h_{ij}}+2\mathrm{R_j}\mathrm{h_{ij}}+4\mathrm{R_i}\mathrm{R_j}} + \ln\frac{h_{ij}^2+2R_ih_{ij}+2R_jh_{ij}}{h_{ij}^2+2R_ih_{ij}+2R_jh_{ij}+4R_iR_j}\right), \tag{14}$$

where $\mathrm{A_H}$ is the Hamaker constant dependent on the nanoparticle material. In the case of magnetite–magnetite interaction in an aqueous medium $\mathrm{A_H}$ is equal to 3.4×10^{-20} J (≈8.2 k_{B}T, k_{B} is Boltzmann's constant, T is the absolute room temperature equals 300 K) [128]. For gold in an aqueous medium $\mathrm{A_H}$ equals 6.0×10^{-20} J (≈14.5k_{B}T, T = 300 K) [127]. $\mathrm{R_i}$, $\mathrm{R_j}$ are the radii of interacting nanoparticles, $\mathrm{h}_{ij} = r - (\mathrm{R_i}+\mathrm{R_j})$ is the interparticle gap. For the paired interaction of gold and magnetite nanoparticles, the Hamaker constant can be roughly estimated as the geometric mean [128] of the two values for both materials. The van der Waals attraction force $(\mathbf{F}_{\mathrm{vdw}})_i$ is

$$(\mathbf{F}_{\mathrm{vdw}})_i = -\frac{\partial(U_{\mathrm{vdw}})_{ij}}{\partial \mathbf{r}_i}. \tag{15}$$

According to the Smoluchowski's theory, an estimate of the half coagulation time, at which the number of particles in the system, including composite ones, is halved, is determined by the formula

$$\theta = \frac{6\eta \mathrm{R_m}}{4\rho\nu_0 k_{\mathrm{B}}\mathrm{T}}, \tag{16}$$

where ρ is the radius of action of the interparticle attraction forces, ν_0 is the initial nanoparticle concentration [129]. Estimates show that for the nanoparticle concentration $\nu_0 = 3,2\times10^{16}\ \mathrm{m}^{-3}$ the value of θ is equal to 2.166 s.

It should be noted that the aggregation of MNPs can occur not only during a half-period of an alternating magnetic field but also during each of the half-periods during an extended field action—tens of seconds or even hours, as in an actual experiment.

2.4. The effect of thermal fluctuations on the magnetic properties of the single-domain nanoparticles

One of the key issues related to the use of the single-domain MNPs is their ability to preserve their intrinsic magnetic dipole moment because only in this case the particles can effectively interact with the external magnetic field and have an effective mechanical effect on the membranes of the malignant cells and their mechanoreceptors *in vitro* and *in vivo*.

If the size of ferrimagnetic magnetite nanoparticles ($2\mathrm{R_m}$) lies in the range exceeding 20–25 nm and not exceeding 80 nm, it corresponds to the condition of a single domain [7, 130]. This ensures that magnetic ordering and homogeneous magnetization are preserved until saturation along the selected direction in the crystal lattice. A magnetite nanoparticle diameter of less than 25 nm is responsible for the gradual transition from ferrimagnetic to the superparamagnetic state [131]. However, even at half the size, under certain conditions, the particles can retain the ferrimagnetic state if they are a part of the multiparticle aggregates.

Among the important issues related to the use of single-domain magnetite nanoparticles in biomedical applications are their ability to preserve their own magnetic dipole moment **M**, which ensures the effective interaction of nanoparticles with the magnetic field. In turn, this interaction is the basis for the mechanical effect on the cell membrane and mechanoreceptors of the cell.

The problem may be that, under certain conditions, magnetite nanoparticles, as ferrimagnetic as noted above, can

transition to the superparamagnetic state and lose their intrinsic magnetic moment. The magnetic moment of a particle can change its direction as a result of thermal fluctuations. If the characteristic time between such thermally induced switching is significantly shorter than the time during which the particle must make the translational-rotational motion necessary for mechanical action on the membrane, the effective mechanical moment will be reduced as a result of fluctuations in the direction of the magnetic moment.

Let us estimate the characteristic time between thermally induced switchings **M** in magnetite nanoparticles. The average time in which the magnetic moment of the particle will perform thermally induced remagnetization is [132]

$$\tau = \tau_0 \cdot \exp[\mathrm{KV_m}/(k_\mathrm{B}\mathrm{T})]. \tag{17}$$

Here $\tau_0 \sim 10^{-9} \div 10^{-11}$ s. The magnetic anisotropy constant of magnetite nanoparticles (K) depends on their size ($V_m = \pi D_m^3/6$, where V_m is the MNP volume and D_m is its diameter) and is usually evaluated as:

$$\mathrm{K} = \mathrm{K_V} + 6 \cdot \mathrm{K_S}/\mathrm{D_m}, \tag{18}$$

where K_V and K_S are constants of volumetric and surface anisotropy, respectively. The values of these constants can vary widely depending on the degree of defects, deviation from stoichiometry, and surface conditions. However, for particles larger than 5 nm, the value of K is always higher than the anisotropy constant of a bulk magnetite monocrystal.

According to [133–137] $K_V = 2.1 \times 10^4\ \mathrm{J\,m^{-3}}$ and $K_S = 2.9 \times 10^{-5}\ \mathrm{J\,m^{-2}}$. We estimate the magnetization reversal times (τ) (at temperature $T = 310\,K = 273\,K + 37\,K$) for magnetite nanoparticles with sizes (see figure 7(b)) corresponding to experiments [13].

According to our calculations, the time of motion of the magnetite particle from the initial position to the moment of alignment of its magnetic moment is from several tens of microseconds (in high-frequency fields) to tens of milliseconds (in low-frequency fields with a frequency of 50 Hz). Hence, the sample contains both particles where thermal fluctuations will decrease the effective magnetic moment (less than 12 nm) and particles where this effect can be neglected (greater than 12 nm), and the number of such particles, according to the histogram of particle size distribution, is at least 30%.

Equation (4) allows us to give an estimate of the acting force from a single isolated particle (figure 2). In the experiment with particles simulated in the present work, the magneto-mechanical effect on the cell membrane is not produced by an isolated particle but by a rigid aggregate of many magnetite nanoparticles connected with a gold nanoparticle. In this case, the gold nanoparticle may be an aggregate element of magnetite nanoparticles bound together by the van der Waals forces. In this case, the chemical bonding of magnetite and gold particles seems unlikely [138]. The formation of such aggregates has been demonstrated by the Brownian dynamics simulations using realistic interparticle potentials [126].

It should be noted that the formation of a large aggregate of MNPs leads, first, to a significant increase in the total magnetic moment of the magneto-mechanical functional unit and hence to an increase in the rotational momentum, which increases the pulling force on the membrane. Second, it increases the potential barrier to remagnetization, i.e. it will result in a drastic weakening of the thermal fluctuation effect (see e.g. [134, 139]). In this case, the effect of thermal fluctuations of magnetization on the dynamics of a multiparticle aggregate with a magnetically ordered arrangement of the magnetic dipoles of the nanoparticles included in the aggregate can be regarded as insignificant.

3. Nanomaterials applied for experimental studies and their characterization

First of all, let us consider the composition of the hydrosols used in the actual experiments and the size of the nanoparticles [13]. Superparamagnetic nanoparticles NITmagoldCit 50 nm (Nanoimmunotech [140]) were used in the experiments. According to the certificate for this commercial product, the hydrosols purchased consisted of a magnetic iron oxide core of about 8–12 nm and a gold layer 30–40 nm thick (50 nm total). In one of the hydrosols with a particle concentration of 3.2×10^{10} particles/ml, the diameter of the gold particles was 51.8 ± 6.1 nm, and the diameter of the magnetite core was 13.6 ± 1.2 nm. Thus, the thickness of the gold shell was $(38.2 \pm 3.5\ \mathrm{nm})/2$.

The MNPs were in sodium citrate solution (water with 5 mM dissolved sodium citrate was used as an interparticle medium). However, as further shown by TEM studies of hydrosols [140], there were also heterogeneous hydrosols among the purchased NITmagoldCit samples that consisted of separate gold and magnetite fractions of nanoparticles that were also used in the experiments [13].

Functionalization of nanoparticles from all types of hydrosols was performed in phosphate buffer containing calcium and magnesium cations. For all experiments, aptamer-functionalized MNPs in a phosphate buffer were used.

It should be noted that thiolation of the nanoparticle surface prior to their functionalization by aptamers can be accompanied by desorption of the potential-determining citrate ions of the EDL and replacement of the EDL by the thiol adsorption layer. But its thickness will be comparable to the thickness of the dense part of EDL, which will not lead to an increase in the spontaneous coagulation rate.

Gold nanoparticles of all types of these hydrosols were subjected to functionalization with aptamers using thiol groups as it is described in [13]. Experiments on magneto-mechanical therapy [13] were subsequently performed also using all types of these hydrosols and the results of these experiments demonstrated a stable reproducibility of high efficiency of the Ehrlich carcinoma therapy.

As noted above, in addition to the classical magnetite core–gold shell nanoparticles, any other combinations of nanoparticles in heterogeneous hydrosols used in experiments must contain both magnetite nanoparticles and gold nanoparticles or gold fragments on the magnetite nanoparticle surface [141–143], examples of which are shown in figure 5. The presence

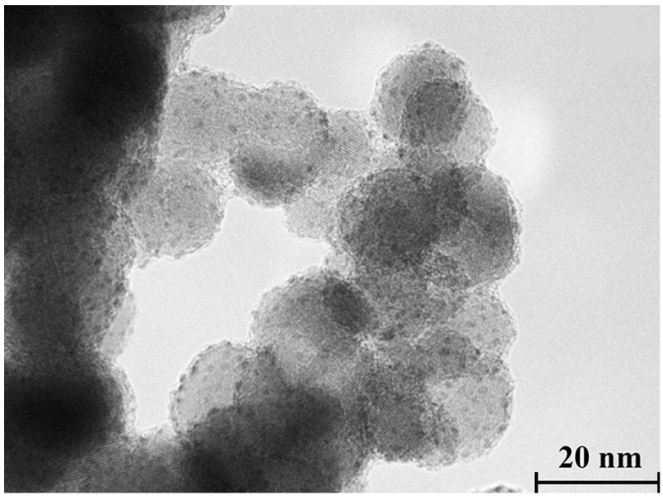

Figure 5. Examples of decorated magnetite nanoparticles with gold nanoclusters on the surface provide the ability to conjugate with aptamers (TEM image). Courtesy of Dr S Saikova.

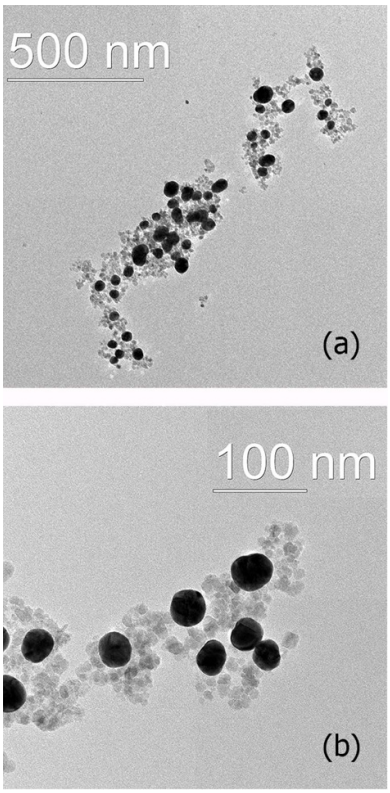

Figure 6. TEM images of gold (dark areas) and magnetite nanoparticles, as well as their aggregates formed in the heterogeneous (gold–magnetite) hydrosols in the process of slow spontaneous aggregation).

of gold particles in the heterogeneous hydrosols or gold fragments (nanoclusters) on the surface of magnetite nanoparticles is mandatory because aptamers can conjugate only to the gold surface.

Figure 6 shows TEM images of particles in the heterogeneous types of hydrosols, which were also used in experiments [13]. Panels A and B show nanoparticles with different

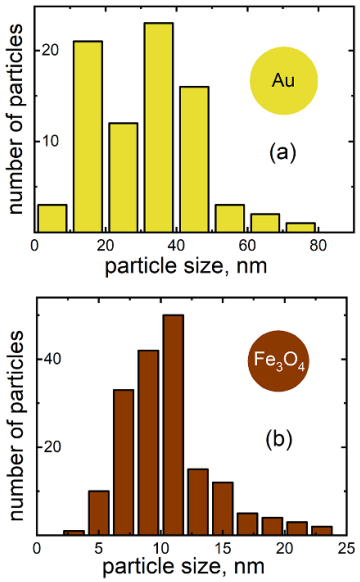

Figure 7. Gold (a) and magnetite (b) nanoparticle size distribution functions in a heterogeneous hydrosol (gold–magnetite) used in the experiment [13] (obtained by averaging 177 particles). The average size of magnetite nanoparticles is 11 nm, and gold nanoparticles are 31 nm.

magnifications. Figure 7 shows histograms of the size distribution of Au and magnetite nanoparticles in this heterogeneous hydrosol obtained using figure 6.

Figure 8 shows the distinctive features of large aggregates of magnetite particles in the hydrosol (Nanoimmunotech [140]) in the absence and in the presence of a magnetic field. In the latter case, the aggregates acquire a strongly elongated shape.

In the absence of a magnetic field, the nanoparticles form disordered aggregates (figure 8(a), under the same conditions in the presence of a magnetic field they line up in chains along the magnetic field (figure 8(b)). The high-affinity aptamer AS-14, specific for the Ehrlich carcinoma cells, attached MNP to the plasma membrane of these cancer cells.

According to laser scanning microscopy analysis, aptamer-modified magnetite–Au nanoparticles formed aggregates arranged in chains around the cell. These chains are marked with white arrows in the figure 9(a) and appear as thin filaments composed of magnetite nanoparticles. Large disordered aggregates of MNPs adhered to cells in the intercellular area (red arrows, figure 9(a)). Ten-minute exposure to an alternating sinusoidal magnetic field of 7958 A m^{-1} at 50 Hz caused apoptosis and further necrosis of the treated cells *in vitro* (figure 9(b)).

Gold-decorated MNPs were stabilized with an high performance liquid chromatography purified oligonucleotide complimentary to the 5′ of aptamer 5′-CGTGGTTACAGTCAGAGGAGAA-/5ThioMC6-D/-3′ modified at the 3′ position with a 6-hydroxyhexyl disulfide group (Integrated DNA Technologies, USA), in the storage buffer for 24 h at 4 °C in a shaker (final concentration of 500 nM). The mixture was

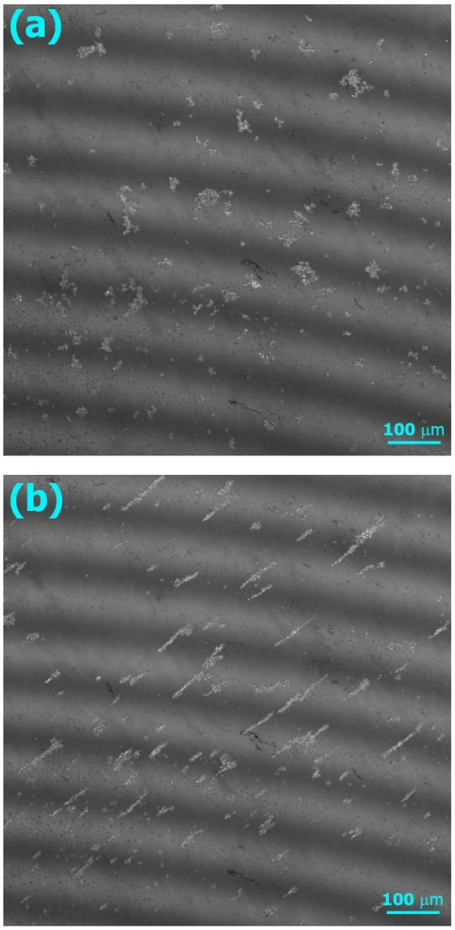

Figure 8. The shape of magnetite multiparticle aggregates: (a)—in the absence of a magnetic field, MNPs form disordered aggregates, (b)—under the same conditions in the presence of a magnetic field, the aggregates form an elongated structure and line up along the field direction. Periodic fringes in images result from interference on two closely spaced glass substrates between which the objects are located. Magnetic nanoparticles Nanoimmunotech [140] in sodium citrate solution.

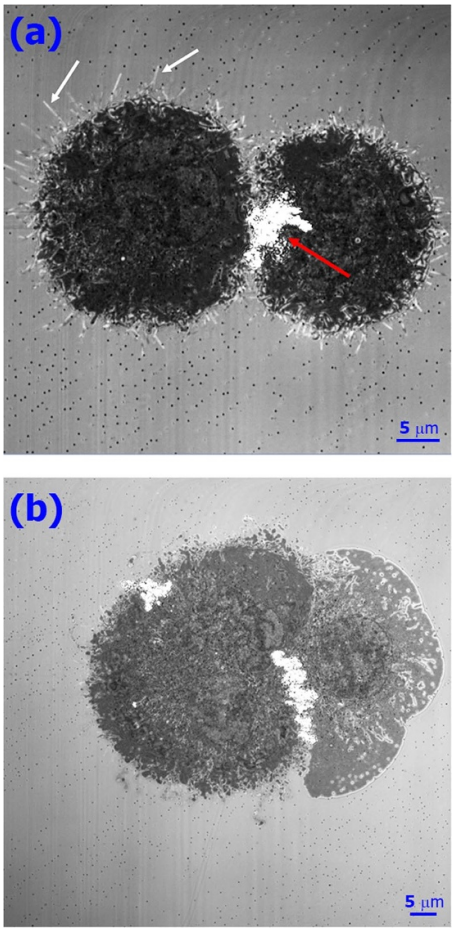

Figure 9. Confocal laser scanning microscopy images of two malignant cells with magnetite nanoparticles on the membrane: (a)—nanoparticle (thin filaments composed of magnetite nanoparticles) formed chain-like structures around the cell surface; (b)—view of cells after 10 min exposure to the alternating magnetic field. Light areas are disordered aggregations of magnetite particles between cells.

diluted 1:1 by mixing it with 2 × DPBS (Dulbecco's phosphate-buffered saline) (with calcium and magnesium) and with an equimolar amount of aptamer AS-14 (5′-TCCTCTGACTGTAACCACGAAGGTGTCGGCCTTAGTAAGGCTACAGCCAAGGGAACGTAGCATAGGTAGTCCAGAAGCC-3′), denatured at 95 °C for 10 min, recovered on ice for 10 min, and incubated for 24 h at 4 °C. The Ehrlich carcinoma cells were incubated in colorless high-glucose calcium and magnesium contained DMEM (Dulbecco's Modified Eagle Medium) with AS-14-MNPs for 30 min at 37 °C in a humidified an atmosphere containing 5% CO2. Cells were washed with the same buffer and were kept in a magnet producing low frequency alternating magnetic field for 10 min. Cell viability was estimated 2 h after the treatment. Confocal microscopy analyses were performed using LSM 780 NLO a model with an additional channel for registering transmitted visible light (Carl Zeiss), ×20, 40 magnification; images were processed with ZEN2 software.

4. Results and discussion

It has been previously demonstrated [13] that 10 min magneto-mechanical therapy with DNA-aptamers functionalized MNPs in the low-frequency alternating magnetic field causes caspase-mediated apoptosis of the Ehrlich carcinoma cells *in vitro* and *in vivo*.

4.1. Kinetics of interaction of a MNP with a cell membrane in an alternating magnetic field

Using the ANSYS Mechanical finite element method in combination with ANSYS Fluent [144], we obtained the results of calculating the vertical component of the force $|\mathbf{F}_n|$ acting on the membrane (at the point of the location of the transmembrane protein) as well as of the velocity of particles (figures 10).

In the experimental conditions, the diameter of gold particles was 30–50 nm, and magnetite particles (or magnetite

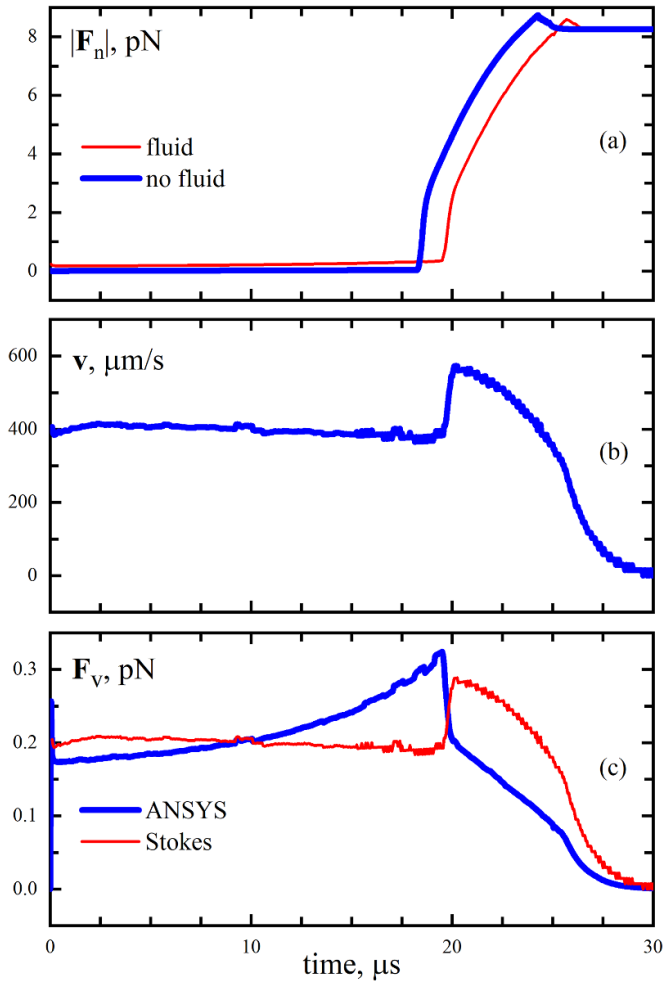

Figure 10. (a)—change in time of the particle's action on the membrane $|\mathbf{F}_n|$ considering its motion in a viscous medium, as well as in the absence of viscosity in a high-frequency magnetic field. The diameter of the gold particle is 30 nm, and the magnetite core is 14 nm. (b)—change in the particle velocity (**v**) over time during a cycle of oscillations in an alternating magnetic field. (c)—change in time of the force of viscous friction ($\mathbf{F}_v$) acting on a nanoparticle that is moving at a velocity **v** is described by Stokes's formula). Comparative calculations are presented made in the ANSYS Fluent package, as well as by the Stokes formula, but using the velocity value obtained from ANSYS Fluent (magnetic field induction is increased to 0.1 T).

core)—11–14 nm. Based on the average value, the membrane thickness was assumed to be 5 nm.

The aptamer bound to fibronectin domain 5 and its fragment between domains 5 and 10 sticks MNP with the membrane through the transmembrane protein, integrin, connected to domain 10 of fibronectin.

The maximum angle between the magnetic field direction and the intrinsic magnetic moment of the particle does not exceed 90°. At the initial moment the particle is located above the integrin and does not touch the membrane.

The following membrane characteristics were used in the calculations: density of 970 kg m^{-3}, the elasticity modulus of 10^5–10^7 Pa, and Poisson's ratio is of 0.4 [145, 146].

The calculation was carried out for the simplified case, the scheme of which is shown in figure 2 with—the motion of a particle bound by an aptamer to a certain point of the membrane. The motion was realized both in a viscous medium (in water) and in a conditional medium in the absence of viscous friction. The time variation of the vertical projection of the force in this geometry, acting on the membrane from the 30 nm diameter core–shell particle with a magnetite core size of 14 nm at a magnetic field induction of 0.1 T, is shown in figure 10(a). Taking into account the proportionality of the magnitude of the field strength, a decrease in the field to experimental values will weaken the force by order of magnitude.

As can be seen from the figure, the contact of the particle with the membrane occurs smoothly, with a slight increase in the force $\mathbf{F}_n$ at the moment of contact ($t = 25\,\mu$s), after which the value of the force tends to the static limit. That is, the time in which the particle makes one oscillation at a constant field action is 25 μs. If the field frequency is 50 Hz as in the [13] experiments, then during the half-period the particle is in a stationary state after touching the membrane.

Since the sizes of magnetite nanoparticles are known and they do not exceed 14 nm (see figure 7), overcoming the problem is related to taking into account the possibility of aggregation of MNPs in the heterogeneous hydrosols used, consisting of gold and magnetite nanoparticles. The centers of aggregation are gold nanoparticles, on which, under the action of short-range van der Waals forces, a minimum number of magnetite seed particles are deposited, which in the magnetic field create conditions for the action of long-range magnetodipole attraction forces. Such aggregation is accompanied by an increase in the effective magnetite volume, by an increase in the total magnetic dipole moment, and by the emergence of conditions for preserving the ferrimagnetic state of nanoparticles with magnetic ordering of neighboring particles.

The change in time of the velocity of the translational motion of a particle in a viscous medium is shown in the figure 10(b). These data were used to calculate the force of viscous friction by the Stokes formula.

Here $\mathbf{v}_i$ is a nanoparticle velocity, R is the nanoparticle radius, and ν is the viscosity of the ambient medium.

The time variation of the viscous frictional force as the particle moves is shown in figure 10(c). The maximum value of this force is reached at the moment of touching the membrane $t = 20\,\mu$s and is 0.32 pN.

4.2. Interaction forces of MNPs with the cell membrane and formation of magnetically ordered nanoparticle aggregates in an alternating magnetic field

Figure 11 shows the results of calculations of the vertical projection of the pulling force ($|\mathbf{F}_n|$) on the membrane by MNP in different geometries: under the action of a single magnetite nanoparticle and a pair of gold and magnetite nanoparticles, as well as 'magnetite core–gold shell nanoparticle', depending on the core size and shell thickness.

As can be seen from this figure, at the field strength used in the experiments, the value of the force $\mathbf{F}_n$ acting on the membrane is much lower than the threshold value (4 pN) [100] at

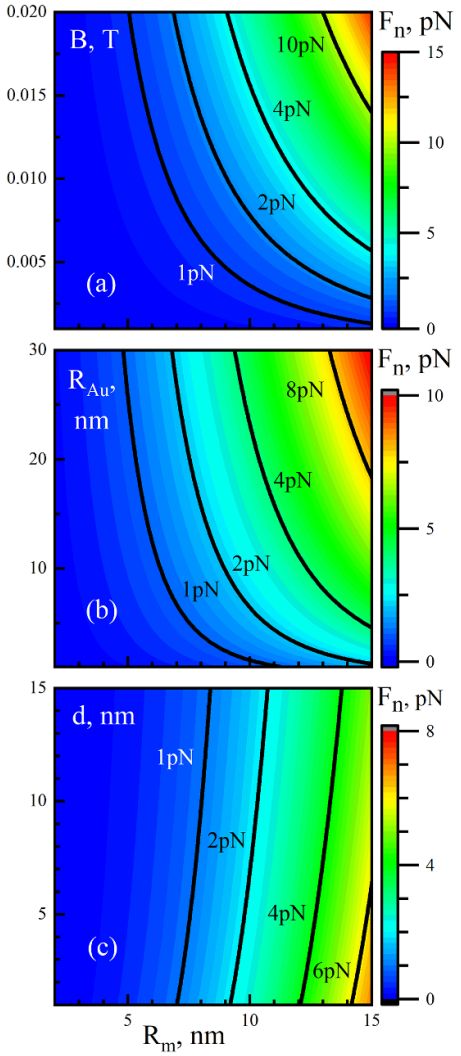

Figure 11. (a)—maximum value of the vertical projection of the pulling force (F_n) acting on the membrane from the magnetite particle vs a magnetic field induction (**B**). R_m is the effective radius of the magnetite particle calculated using the formula (4), (b)—the maximal value of the force acting on the membrane from a pair of bound particles—gold nanoparticle bound to the membrane and magnetite nanoparticle (calculated using the formula (5)); (c)—maximal value of the force acting on the membrane from a core–shell nanoparticle. d is the thickness of the gold shell (calculated using the formula (6)). In cases (b) and (c), the field strength $\mathbf{H} = 7958\ \mathrm{A\,m^{-1}}$ corresponds to the experimental value of magnetic field induction $\mathbf{B} = 0.01$ T.

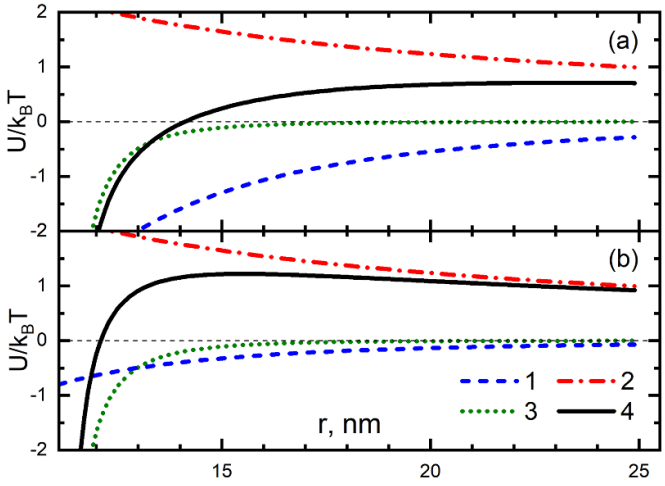

Figure 12. Comparison of the energy (in k_BT units, T = 300 K) of paired interaction of magnetite nanoparticles as a function of the center-to-center distance: (1)—magneto-dipole interaction (equation (8)); (2)—electrostatic interaction of particles stabilized by electric double layers (equation (14)); (3)—the van der Waals interaction (equation (15)) and (4)—the sum of all interactions. (a) is the case of the collinear arrangement of interacting magnetic dipoles along the external magnetic field, (b) is the case of the orientation of the inter-center vector of dipoles at an angle of 60° with respect to the external field direction. Magnetite nanoparticle size is 11 nm.

any variant of the geometry of magnetite particles of the same size, close to the experimental values. This conclusion also follows from a comparison of equations (4)–(6). Exceeding the threshold is possible only in the case of a significant increase in the effective size of MNPs, or in the increase in the magnetic field strength. But in the actual experiment, the therapeutic effect was observed already at small field strengths.

As shown above, the strength of the effect of a single particle on the mechanoreceptors of a malignant cell at experimental values of magnetic field strength is significantly below the threshold strength (4 pN), which is insufficient to trigger apoptosis.

In this connection, it is necessary to study the conditions of magnetically ordered aggregation of MNPs in the magnetic field and the possibility of forming aggregates with a large effective magnetic dipole moment. Such aggregates can consist of magnetite nanoparticles both with a homogeneous structure and 'core–shell' particles.

First of all, let us analyze the pairwise interparticle potentials showing the possibility of particle coagulation. Figure 12 shows different types of interparticle interactions, confirming the possibility of coagulation of nanoparticles in the main potential minimum and the formation of multiparticle aggregates. This figure demonstrates the dependence of the paired interaction energy of magnetite nanoparticles. As follows from the figure, the paired magneto-dipole interactions are much more long-range with the radius of action of the order of 1.5 center-to-center distances (for magnetite particles sized 11 nm) compared to the short-range van der Waals forces.

Figure 13 demonstrates elongated aggregates of magnetite particles in the presence of a magnetic field involving a gold nanoparticle bioconjugate. The structure was obtained by the Brownian dynamics simulation method using formulas for the paired inter-particle interaction energy presented in section 2.3, taking into account the stochastic force [122].

The formation of rigid nanoparticle aggregates that retain their spatial structure is accompanied by an increase in the total magnetic moment, which is proportional to the total volume of all magnetite particles in the aggregate.

In experimental conditions, this is clearly demonstrated in figure 8, which shows the cardinal difference in the shape of large aggregates of magnetite particles in the hydrosol in the absence and presence of a magnetic field.

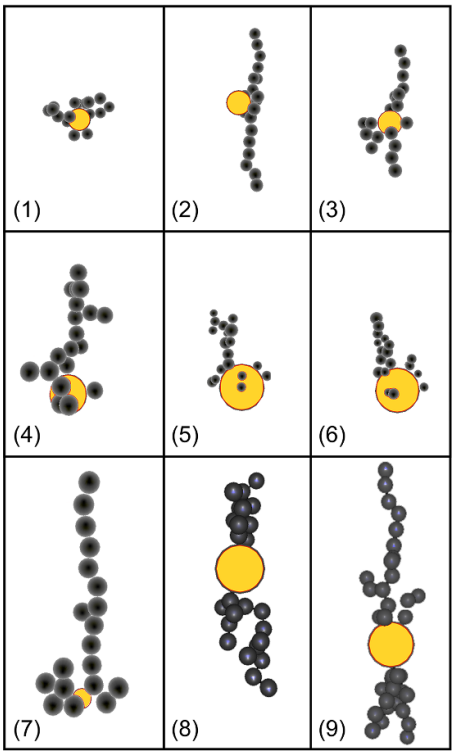

Figure 13. The structure of aggregates formed during the van der Waals interaction of magnetite nanoparticles with gold nanoparticles and with each other taking into account the paired magneto-dipole interaction of particles of the same size in the magnetic field. (1)—under spontaneous aggregation conditions in the absence of a magnetic field (magnetite particle size is of 14.6 nm, gold particle size is of 30 nm); (2, 3)—aggregation in the presence of a magnetic field; (4)—the result of aggregation of 14 nm magnetite particles with the 2 nm gold shell thickness on a 40 nm gold particle; (5, 6)—aggregation of polydisperse magnetite particles having an average size of 11 nm with the gold particle size of 40 nm (particle size distribution corresponds to the experimental data in figure 6); (7)—the result of aggregation of particles with a magnetite core of 30 nm with the gold shell thickness of 5 nm (the lower particle is highlighted by color is fixed on the membrane); (8, 9)—aggregates of 14.6 nm magnetite particles formed with a gold particle with a magnetite core of 50 nm (geometry according to figure 4). In figures (2)–(9), the formation of aggregates occurs in the presence of a magnetic field (field direction is vertical—along the anisotropy axis of the aggregates.

The irregular shape of the magnetite particles (see figure 6), which prevents the particles from sliding on each other, and provides a high rigidity of the aggregate. The number of magnetite particles deposited on the gold can greatly exceed several dozen.

Aggregates shown in figure 13 are the results of simulations of the nanoparticle coagulation in a heterogeneous hydrosol consisting of ferrimagnetic nanoparticles, which possess their intrinsic magnetic dipole moment in the presence of an external magnetic field. The purpose of this simulation is to establish the possibility of accumulation of total magnetic moment by a rigid aggregate of magnetite particles to increase its response to an external magnetic field. As can be seen from the figure, the structure of aggregates in such a system, consisting of a rigid gold particle fixed on a plane (simulating the membrane) and smaller magnetite particles, are characterized by a strongly extended, chain-like structure. It arises due to the interaction of magnetic moments of each particle with each other in conditions of co-directionality of their dipole moments. Under the action of an external magnetic field, magnetite particles line up collinearly and tend to form an elongated aggregate oriented along the field. Paired interaction of such particles includes both long-range magneto-dipole interaction and short-range van der Waals interaction, which appears when the particles approach a short distance (the radius of action of the van der Waals forces), primarily magnetite particles to gold. In this case, the van der Waals interaction of magnetite particles with the gold particle dominates in comparison with the van der Waals interaction of the magnetite particles themselves with each other due to the significant difference in the Hamaker constants for these materials.

Deposition of magnetite nanoparticles occurs on the gold particle bound to the transmembrane protein. As can be seen from figure 13(1), if the magneto-dipole interactions of the particles are turned off, the aggregation of magnetite particles onto the gold particle appears chaotic and resembles the formation of normal disordered colloidal aggregates. Clear evidence of this is a comparison of figure 13(1, 2, 3) and figure 8. Figure 13(7, 8, 9) shows the structure of the core–shell type aggregates, and aggregates composed of magnetite and gold nanoparticles.

As the particle size decreases, the structure of the aggregates becomes less ordered with a gradual deterioration of the degree of orientational ordering and the aggregates gradually lose their elongated structure.

Strongly anisotropic aggregates of magnetite particles formed under experimental conditions in an aqueous medium in the presence of a magnetic field are shown for comparison in figure 8.

Tendencies to the formation of a chain structure in the aggregation of magnetite particles in size are also observed in the polydisperse heterogeneous hydrosol during their deposition on gold nanoparticles.

As can be seen from figure 8, the tendency to form elongated aggregates from magnetite particles is being manifested under conditions of a magnetic field. It is shown that quite a large number of magnetite particles are deposited on the gold particle, the volume of which can be at least ten times greater than the volume of a single magnetite particle. It is also important to note that due to the complex shape of such particles, which is very different from spherical, the structure of aggregates is rigid and is preserved when the field direction is changed. In this case, if the force of the action of a single particle on the transmembrane protein was insufficient and did not exceed the threshold value at the experimental amplitude of the alternating magnetic field strength, the aggregate of such magnetite particles, or of nanoparticles with a magnetite core and gold shell, will interact much more efficiently with the membrane under the influence of the external magnetic field. The number of magnetite particles that can be deposited on the gold particle can significantly exceed the limit determined by the surface area of the gold particle for monolayer

coagulation. In this case, the total magnetic dipole moment of a large aggregate will be dozens of times greater than the magnetic moment of a single particle.

Thus, an important conclusion of this stage of research is that, by taking into account aggregation, it is possible to achieve and exceed the threshold value of the force acting on the transmembrane protein of a gold nanoparticle surrounded by a multiparticle structure of magnetite particles. This cumulative effect on the mechanoreceptor becomes sufficient to trigger apoptosis in weak non-heating alternating magnetic fields.

5. Conclusion

In our paper, we applied numerical simulations to explain the experimental results on targeted magneto-mechanical tumor therapy with MNPs obtained in the paper [13]. In this work, malignant Ehrlich's carcinoma tissue cells were effectively killed by MNPs functionalized with aptamers as recognition markers in the non-heating alternating magnetic field.

The principal tool of impact on the malignant cells in low-frequency magnetic fields are MNPs functionalized with aptamers or other agents that recognize malignant tissue markers.

Aptamer selection makes it possible to create nanoparticle bioconjugates capable of selectively binding to the cell membranes of any type of malignancies, including epithelial cells, which are related to the experimental results discussed in our paper.

The targeted effect of nanoparticles on the membranes of malignant cells, with which MNPs bind, is carried out by mechanical rotation of nanoparticles in an alternating magnetic field with a periodic change of the field direction.

The connection of the MNP with the membrane elements during rotation leads to a mechanical impact on the cell mechanoreceptors. This results in an emergence of a vertical (to the outer surface of the membrane) projection of the pulling force through the chain of consecutive arranged elements: aptamer—fibronectin—integrin (as a transmembrane mechanoreceptor).

The results of our work allow us to make the following statements:

(a) Based on the information in the literature regarding the mechanisms of the triggering of the programmed death of malignant cells (apoptosis), we can argue about the possibility of achieving, under actual experimental conditions, a mechanical effect on the transmembrane protein with force exceeding the threshold value—from 4 to 10 pN.

(b) Realization of mechanical influence mechanisms is possible through different configurations of superparamagnetic nanoparticles and may include particles with magnetic core and gold shell, dimers consisting of gold and MNPs, but provided that the minimum allowed particle volume is exceeded to ensure the achievement of the threshold influence.
In addition, magnetite nanoparticles with moderate biocompatibility, decorated with gold clusters, with which aptamers can conjugate and perform targeted binding to the malignant cells, can also affect the membrane.

(c) When implementing magneto-mechanical therapy using MNPs, preference should be given to superparamagnetic nanoparticles, since they exhibit magnetic properties only when a magnetic field is applied. In the absence of a field, the magnetic moment of superparamagnetic nanoparticles is equal to zero. This feature prevents the fast spontaneous aggregation of superparamagnetic nanoparticles in the absence of a magnetic field.

(d) It is shown that the impact on the cell mechanoreceptors to trigger apoptosis, estimated by the force threshold value exceeding 4 pN, is impossible through single magnetite superparamagnetic nanoparticles sized 11–14 nm under the conditions corresponding to the experimental data. The method of Brownian dynamics using realistic pair potentials shows that magnetite particles, preserving the intrinsic magnetic dipole moment in the magnetic field can form multiparticle anisotropic aggregates due to long-range dipole–dipole interactions and attach to condensation centers, which are bioconjugates of gold nanoparticles linked to the membrane mechanoreceptors.

(e) The formation of aggregates from orientationally ordered superparamagnetic magnetite nanoparticles around a gold particle in the magnetic field is accompanied by the following consequences:
   1. suppression of thermal fluctuations of the magnetic dipole moment in single superparamagnetic nanoparticles, taking into account the fact that the conservation of the magnetic dipole moment in single magnetite particles is possible with their sizes exceeding 20–25 nm. Additional interactions of the magnetic moments of nanoparticles under conditions of their orientational ordering create a collective magnetic field, which significantly increases the magnetization reversal barrier of superparamagnetic magnetite nanoparticles of smaller size, suppresses thermal fluctuations, and makes it possible to preserve the amplitude and direction of the magnetic dipole moment of the particles, which actually gives them ferrimagnetic properties;
   2. an increase in the total magnetic dipole moment of the aggregate, which contributes to an increase in the force of action on the membrane mechanoreceptor, significantly exceeding the threshold value.

   The aggregation effect of MNPs is possible in any system of nanoparticles used for magneto-mechanical anticancer therapy and allows predicting an increase in the impact on the malignant cells.

(f) The information obtained in our work using the dynamic simulation model makes it possible to provide an explanation for the experimental facts demonstrated in work [13], which confirmed that the magneto-mechanical therapy based on magnetite nanoparticles with a gold shell or with gold fragments on the nanoparticle surface results in the

destruction of the Ehrlich carcinoma *in vivo* and *in vitro* in a non-heating alternating magnetic field.

The obtained results confirm the possibility of the successful application of the method for the highly effective treatment of malignant neoplasms and open up the prospects for its implementation in medical practice.

Data availability statement

All data that support the findings of this study are included within the article (and any supplementary files).

Acknowledgment

P N S, A S K, D E K, S P P, S V K acknowledge the support by the Ministry of Science and High Education of Russian Federation (Project No. FSRZ-2020-0008). Experimental analyses were funded by the Ministry of Science and Higher Education of the Russian Federation (Project FWES-2022-0005) – A S K, T N Z. The authors thank Dr S V Saikova for providing the TEM image in figure 5(b).

Conflicts of interest

There are no conflicts of interest to declare.

ORCID iDs

I L Isaev https://orcid.org/0000-0001-5438-0684
S V Komogortsev https://orcid.org/0000-0002-2686-3643
A B Klyuchantsev https://orcid.org/0000-0003-4362-588X
A S Kichkailo https://orcid.org/0000-0003-1054-4629
T N Zamay https://orcid.org/0000-0002-7493-8742
I N Lapin https://orcid.org/0000-0001-5736-3791
S P Polyutov https://orcid.org/0000-0003-1366-1986
S V Karpov https://orcid.org/0000-0002-5170-1697

References

[1] Chen X, Gambhir S S and Cheon J 2011 *Acc. Chem. Res.* **44** 841
[2] Kim T H, Lee S and Chen X 2013 *Expert Rev. Mol. Diagn.* **13** 257–69
[3] Ryu J H, Lee S, Son S, Kim S H, Leary J F, Choi K and Kwon I C 2014 *J. Control. Release* **190** 477–84
[4] Muthu M S, Leong D T, Mei L and Feng S S 2014 *Theranostics* **4** 660–77
[5] Lim E K, Kim T, Paik S, Haam S, Huh Y M and Lee K 2014 *Chem. Rev.* **115** 327–94
[6] Kunjachan S, Ehling J, Storm G, Kiessling F and Lammers T 2015 *Chem. Rev.* **115** 10907–37
[7] Golovin Y I *et al* 2018 *Nanotechnol. Russia* **13** 215–39
[8] Banerjee R, Katsenovich Y, Lagos L, McIintosh M, Zhang X and Li C Z 2010 *Curr. Med. Chem.* **17** 3120–41
[9] Dreaden E C, Alkilany A M, Huang X, Murphy C J and El-Sayed M A 2012 *Chem. Soc. Rev.* **41** 2740–79
[10] Gu F X, Karnik R, Wang A Z, Alexis F, Levy-Nissenbaum E, Hong S, Langer R S and Farokhzad O C 2007 *Nano Today* **2** 14–21
[11] Liu Q, Jin C, Wang Y, Fang X, Zhang X, Chen Z and Tan W 2014 *NPG Asia Mater.* **6** e95–e104
[12] Malik M T, O'Toole M G, Casson L K, Thomas S D, Bardi G T, Reyes-Reyes E M, Ng C K, Kang K A and Bates P J 2015 *Oncotarget* **6** 22270–81
[13] Belyanina I V *et al* 2017 *Theranostics* **7** 3326–37
[14] Golovin Y I, Klyachko N L, Majouga A G, Sokolsky M and Kabanov A V 2017 *J. Nanopart Res.* **19** 63
[15] Shen Y, Wu C, Uyeda T Q P, Plaza G R, Liu B, Han Y, Lesniak M S and Cheng Y 2017 *Theranostics* **7** 1735–48
[16] Golovin Y I, Gribanovsky S L, Golovin D Y, Zhigachev A O, Klyachko N L, Majouga A G, Sokolsky M and Kabanov A V 2017 *J. Nanoparticle Res.* **19** 59
[17] Golovin Y I, Zhigachev A O, Klyachko N L and Kabanov A V 2018 *Bull. Russ. Acad. Sci.: Phys.* **82** 1073–8
[18] Abdel-Mohsen M A, El-Braky A A A, Ghazal A A E R and Shamseya M M 2018 *Medicine* **97** e0172–8
[19] Naud C, Thébault C, Carrière M, Hou Y, Morel R, Berger F, Diény B and Joisten H 2020 *Nanoscale Adv.* **2** 3632–55
[20] Muzzi B *et al* 2022 *ACS Appl. Mater. Interfaces* **14** 29087–98
[21] Gerasimov V S, Ershov A E, Karpov S V, Polyutov S P and Semina P N 2016 *Colloid J.* **78** 435–42
[22] Kolovskaya O S *et al* 2017 *Mol. Ther. Nucleic Acids* **9** 12–21
[23] Kostyukov A S, Ershov A E, Gerasimov V S, Filimonov S A, Rasskazov I L and Karpov S V 2019 *J. Quant. Spectrosc. Radiat. Transfer* **236** 106599–628
[24] Bienia A, Wiecheć-Cudak O, Murzyn A A and Krzykawska-Serda M 2021 *Pharmaceutics* **13** 1147–94
[25] Lapotko D O, Lukianova E and Oraevsky A A 2006 *Lasers Surg. Med.* **38** 631–42
[26] Zharov V P, Mercer K E, Galitovskaya E N and Smeltzer M S 2006 *Biophys. J.* **90** 619–27
[27] Galanzha E I *et al* 2019 *Sci. Trans. Med.* **11** eaat5857–69
[28] Kostyukov A S, Isaev I L, Ershov A E, Gerasimov V S, Polyutov S P and Karpov S V 2022 *J. Phys. D: Appl. Phys.* **55** 175401
[29] Kostyukov A S, Isaev I L, Ershov A E, Gerasimov V S, Polyutov S P and Karpov S V 2022 *J. Phys. D: Appl. Phys.* **55** 175402
[30] Ershov A E, Gerasimov V S, Gavrilyuk A P and Karpov S V 2017 *Appl. Phys.* B **123** 182–91
[31] Gerasimov V S, Ershov A E, Karpov S V, Gavrilyuk A P, Zakomirnyi V I, Rasskazov I L, Ågren H and Polyutov S P 2017 *Opt. Mater. Express* **7** 555–68
[32] Sørensen L K *et al* 2022 *Nanoscale* **14** 433–47
[33] Baraton M I (ed) 2002 *Synthesis, Functionalization and Surface Treatment of Nanoparticles*, (Stevenson Ranch, CA: American Scientific)
[34] Zamay T N, Prokopenko V S, Zamay S S, Lukyanenko K A, Kolovskaya O S, Orlov V A, Zamay G S, Galeev R G, Narodov A A and Kichkailo A S 2021 *Nanomaterials* **11** 1459–73
[35] Zamay G S, Zamay T N, Lukyanenko K A and Kichkailo A S 2020 *Biomedicines* **8** 59–72
[36] Golovin Y I, Gribanovsky S L, Golovin D Y, Klyachko N L, Majouga A G, Master A M, Sokolsky M and Kabanov A V 2015 *J. Control. Release* **219** 43–60
[37] Tuerk C and Gold L 1990 *Science* **249** 505–10
[38] Ellington A D and Szostak J W 1990 *Nature* **346** 818–22
[39] Nimjee S M, Rusconi C P and Sullenger B A 2005 *Annu. Rev. Med.* **56** 555–83
[40] Aljohani M M, Cialla-May D, Popp J, Chinnappan R, Al-Kattan K and Zourob M 2022 *Molecules* **27** 383–403
[41] Singh N, Jenkins G J, Asadi R and Doak S H 2010 *Nano Rev.* **1** 5358–72

[42] Fang C and Zhang M 2009 *J. Mater. Chem.* **19** 6258–66
[43] Challa S S (ed) 2005 *Biofunctionalization of Nanomaterials* (*Nanotechnologies for the Life Sciences*) (Weinheim: Wiley-VCH Verlag)
[44] Venugopal I, Pernal S, Duproz A, Bentley J, Engelhard H and Linninger A 2016 *Mater. Res. Express* **3** 095010–22
[45] Gholami A, Mousavi S M, Hashemi S A, Ghasemi Y, Chiang W H and Parvin N 2020 *Drug Metab. Rev.* **52** 205–23
[46] Majee S and Shit G 2020 *Eur. J. Mech.* B **83** 42–57
[47] Colombo M, Carregal-Romero S, Casula M F, Gutiérrez L, Morales M P, Böhm I B, Heverhagen J T, Prosperi D and Parak W J 2012 *Chem. Soc. Rev.* **41** 4306–34
[48] Lübbe A, Bergemann C, Huhnt W, Fricke T, Riess H, Brock J and Huhn D 1996 *Cancer Res.* **56** 4694–701
[49] Iancu S D, Albu C, Chiriac L, Moldovan R, Stefancu A, Moisoiu V, Coman V, Szabo L, Leopold N and Bálint Z 2020 *Int. J. Nanomed.* **15** 4811–24
[50] Avasthi A, Caro C, Pozo-Torres E, Leal M P and García-Martín M L 2020 *Top. Curr. Chem.* **378** 40–82
[51] Zhao Z, Cui H, Song W, Ru X, Zhou W and Yu X 2020
[52] Wang Z, Cheng L, Sun Y, Wei X, Cai B, Liao L, Zhang Y and Zhao X Z 2020 *Anal. Chem.* **93** 1033–42
[53] Tang C *et al* 2020 *J. Nanobiotechnology* **18** 62–84
[54] Zhang Z 2020 *J. Phys.: Conf. Ser.* **1699** 012007
[55] Kim D, Lee Y D, Jo S, Kim S and Lee T S 2020 *Sens. Actuator* B **307** 127641
[56] Stolyar S V, Komogortsev S V, Gorbenko A S, Knyazev Y V, Yaroslavtsev R N, Olkhovskiy I A, Neznakhin D S, Tyumentseva A V, Bayukov O A and Iskhakov R S 2022 *J. Supercomput. Novel Magn.* **35** 1929–36
[57] Sosa-Acosta J R, Iriarte-Mesa C, Ortega G A and Díaz-García A M 2020 *Top. Curr. Chem.* **378** 13–41
[58] Fatima H and Kim K S 2017 *Korean J. Chem. Eng.* **34** 589–99
[59] Yang Q, Dong Y, Qiu Y, Yang X, Cao H and Wu Y 2020 *Colloids Surf.* B **191** 111014–66
[60] Kerativitayanan P, Carrow J K and Gaharwar A K 2015 *Adv. Healthcare Mater.* **4** 1600–27
[61] Lee K, Yi Y and Yu Y 2016 *Angew. Chem., Int. Ed.* **55** 7384–7
[62] Gauger A J, Hershberger K K and Bronstein L M 2020 *Front. Chem.* **8** 561–7
[63] Yoo D, Lee J H, Shin T H and Cheon J 2011 *Acc. Chem. Res.* **44** 863–74
[64] Angelakeris M 2017 *Biochim. Biophys. Acta* **1861** 1642–51
[65] Chen L, Chen C, Wang P and Song T 2017 *J. Nanomater.* **2017** 1–13
[66] Wu Y, Lu Z, Li Y, Yang J and Zhang X 2020 *Nanomaterials* **10** 1441–61
[67] Torchilin V (ed) 2020 *Handbook of Materials for Nanomedicine* (New York: Jenny Stanford Publishing) (https://doi.org/10.1201/9781003045076)
[68] Nuzzo S, Brancato V, Affinito A, Salvatore M, Cavaliere C and Condorelli G 2020 *Cancers* **12** 2173–89
[69] Adachi T and Nakamura Y 2019 *Molecules* **24** 4229–42
[70] Song K M, Lee S and Ban C 2012 *Sensors* **12** 612–31
[71] Sefah K, Shangguan D, Xiong X, O'Donoghue M B and Tan W 2010 *Nat. Protocols* **5** 1169–85
[72] Ouyang L, Shi Z, Zhao S, Wang F T, Zhou T T, Liu B and Bao J K 2012 *Cell Prolif.* **45** 487–98
[73] Barczyk M, Carracedo S and Gullberg D 2009 *Cell Tissue Res.* **339** 269–80
[74] Lutay N V, Brazaluk A Z, Peleshenco A B and Shevtsova A I 2004 *Biopolym. Cell* **20** 402–9
[75] Dolhikh H, Netronina O, Maslak H and Abraimova O 2018 *Lab. Diagn. East. Eur.* **7** 342–59
[76] Danen E H, Sonneveld P, Sonnenberg A and Yamada K M 2000 *J. Cell Biol.* **151** 1413–22
[77] Manabe R, Ohe N, Maeda T, Fukuda T and Sekiguchi K 1997 *J. Cell Biol.* **139** 295–307
[78] Lee E J, Ahmad K, Pathak S, Lee S, Baig M H, Jeong J H, Doh K O, Lee D M and Choi I 2021 *Int. J. Mol. Sci.* **22** 3042–58
[79] Tsaplina O A 2020 *Tsitologiya* **62** 349–55
[80] van der Flier A and Sonnenberg A 2001 *Cell Tissue Res.* **305** 285–98
[81] Legate K R and Fässler R 2009 *J. Cell Sci.* **122** 187–98
[82] Legate K R, Wickström S A and Fässler R 2009 *Genes Dev.* **23** 397–418
[83] Su Y, Xia W, Li J, Walz T, Humphries M J, Vestweber D, Caba nas C, Lu C and Springer T A 2016 *Proc. Natl Acad. Sci.* **113** E3872–81
[84] Chen Y, Lee H, Tong H, Schwartz M and Zhu C 2017 *Matrix Biol.* **60–61** 70–85
[85] Lavrik I, Golks A and Krammer P H 2005 *J. Cell Sci.* **118** 265–7
[86] Dickens L S, Powley I R, Hughes M A and MacFarlane M 2012 *Exp. Cell Res.* **318** 1269–77
[87] Walczak H 2013 *Cold Spring Harb. Perspect. Biol.* **5** a008698–715
[88] Puchinskaya M V 2016 *Arkhiv Patol.* **78** 47–54
[89] Leulmi S *et al* 2015 *Nanoscale* **7** 15904–14
[90] Gorban' N A, Popov A M and Karyakin O B 2016 *Cancer Urol.* **12** 40–43
[91] Deev R, Bilyalov A and Zhampeisov T 2018 *Genes Cells* **XIII** 6–20
[92] Parrish A B, Freel C D and Kornbluth S 2013 *Cold Spring Harb. Perspect. Biol.* **5** a008672–96
[93] Ivanisenko N and Lavrik I N 2019 *Mol. Biol.* **53** 830–7
[94] Wang Z, Liu Y and Cui Y 2005 *Cell Biol. Int.* **29** 489–96
[95] Chen D L, Engle J T, Griffin E A, Miller J P, Chu W, Zhou D and Mach R H 2014 *Mol. Imaging Biol.* **17** 384–93
[96] Palmerini F, Devilard E, Jarry A, Birg F and Xerri L 2001 *Hum. Pathol.* **32** 461–7
[97] Dyatlova A S 2018 *Achievem. Mod. Biol.* **32** 126–37
[98] Puklin-Faucher E, Gao M, Schulten K and Vogel V 2006 *J. Cell Biol.* **175** 349–60
[99] Zhang Y, Chen M, Venugopal S, Zhou Y, Xiang W, Li Y H, Lin Q, Kini R M, Chong Y S and Ge R 2011 *Cell Death Dis.* **2** e153–62
[100] Kilinc D, Lesniak A, Rashdan S A, Gandhi D, Blasiak A, Fannin P C, von Kriegsheim A, Kolch W and Lee G U 2014 *Adv. Healthcare Mater.* **4** 395–404
[101] Kilinc D, Dennis C L and Lee G U 2016 *Adv. Mater.* **28** 5672–80
[102] Roca-Cusachs P, Conte V and Trepat X 2017 *Nat. Cell Biol.* **19** 742–51
[103] Iijima N, Sato K, Kuranaga E and Umetsu D 2020 *Nat. Commun.* **11** 6320–31
[104] Guadamillas M C, Cerezo A and del Pozo M A 2011 *J. Cell Sci.* **124** 3189–97
[105] Baker E L and Zaman M H 2010 *J. Biomech.* **43** 38–44
[106] Campbell I D and Humphries M J 2011 *Cold Spring Harb. Perspect. Biol.* **3** a004994–5008
[107] Takagi J and Springer T A 2002 *Immunol. Rev.* **186** 141–63
[108] Stupack D G and Cheresh D A 2002 *J. Cell Sci.* **115** 3729–38
[109] Gilmore A P 2005 *Cell Death Differ.* **12** 1473–7
[110] Jarnagin W R, Rockey D C, Koteliansky V E, Wang S S and Bissell D M 1994 *J. Cell Biol.* **127** 2037–48
[111] Vartio T, Laitinen L, Narvanen O, Cutolo M, Thornell L, Zardi L and Virtanen I 1987 *J. Cell Sci.* **88** 419–30
[112] Li L *et al* 2012 *J. Nanosci. Nanotechnol.* **12** 9010–17
[113] Bae J E *et al* 2011 *Biomaterials* **32** 9401–14
[114] Minaeva O V *et al* 2017 *J. Phys.: Conf. Ser.* **784** 012038–49
[115] Turanskaya S P, Kusyak A P, Turov V V and Gorbik P P 2013 *Surface* **5** 227–46

[116] Wu Y N, Yang L X, Shi X Y, Li I C, Biazik J M, Ratinac K R, Chen D H, Thordarson P, Shieh D B and Braet F 2011 *Biomaterials* **32** 4565–73
[117] Ozerskaya A V *et al* 2021 *Mol. Ther. Nucleic Acids* **26** 1159–72
[118] Usov N A and Liubimov B Y 2012 *J. Appl. Phys.* **112** 023901
[119] Krafcik A, Babinec P, Strbak O and Frollo I 2021 *Appl. Sci.* **11** 9651
[120] Abramov N V and Gorbik P P 2012 *Surface* **4** 246–65
[121] Lapotko D O, Lukianova-Hleb E Y and Oraevsky A A 2007 *Nanomedicine* **2** 241–53
[122] Ershov A E, Gavrilyuk A P, Karpov S V and Semina P N 2013 *Appl. Phys.* B **115** 547–60
[123] Turkevich J, Stevenson P C and Hillier J 1951 *Discuss. Faraday Soc.* **11** 55–75
[124] Levin Y 2002 *Rep. Prog. Phys.* **65** 1577–632
[125] Frens G 1973 *Nature* **241** 20–22
[126] Gavrilyuk A, Gerasimov V, Ershov A and Karpov S 2018 *Colloid. Polym. Sci.* **296** 1689–97
[127] Hans Sonntag K S 1987 *Coagulation Kinetics and Structure Formation* (New York: Plenum)
[128] Visser J 1972 *Advances in Colloid and Interface Science* **3** 331–63
[129] Karpov S V and Semina P N 2012 *Colloid J.* **74** 295–304
[130] Reichel V *et al* 2017 *Sci. Rep.* **7** 45484–91
[131] Krishnan K M 2010 *IEEE Trans. Magn.* **46** 2523–58
[132] Coffey W T and Kalmykov Y P 2012 *J. Appl. Phys.* **112** 121301–48
[133] Roca A G, Morales M P, O'Grady K and Serna C J 2006 *Nanotechnology* **17** 2783–8
[134] Balaev D, Semenov S, Dubrovskiy A, Yakushkin S, Kirillov V and Martyanov O 2017 *J. Magn. Magn. Mater.* **440** 199–202
[135] Ortega D, Vélez-Fort E, García D A, García R, Litrán R, Barrera-Solano C, del Solar M R and Domínguez M 2010 *Phil. Trans. R. Soc.* A **368** 4407–18
[136] Goya G F, Berquó T S, Fonseca F C and Morales M P 2003 *J. Appl. Phys.* **94** 3520–8
[137] Pérez N, Guardia P, Roca A G, Morales M P, Serna C J, Iglesias O, Bartolomé F, García L M, Batlle X and Labarta A 2008 *Nanotechnology* **19** 475704–12
[138] Sokolov A E, Ivanova O S, Fedorov A S, Kovaleva E A, Vysotin M A, Lin C R and Ovchinnikov S G 2021 *Phys. Solid State* **63** 1536–40
[139] Komogortsev S, Fel'k V and Li O 2019 *J. Magn. Magn. Mater.* **473** 410–5
[140] (Available at: www.nanoimmunotech.eu/en/shop/nanoparticles-/gold-coated-magnetic-nanoparticles)
[141] Saikova S, Trofimova T V, Pavlikov A, Karpov D, Chistyakov D I and Mikhlin Y L 2020 *Russ. Chem. Bull.* **69** 1284–9
[142] Saykova D, Saikova S, Mikhlin Y, Panteleeva M, Ivantsov R and Belova E 2020 *Metals* **10** 1075–87
[143] Saikova S, Pavlikov A, Trofimova T, Mikhlin Yu, Karpov D, Asanova A, Grigoriev Yu, Volochaev M, Samoilo A and Zharkov S 2021 *Metals* **11** 705
[144] Hutton D V 2004 *Fundamentals of Finite Element Analysis Mcgraw-Hill* (*Series in Mechanical Engineering*) (Boston: McGraw-Hill)
[145] Hamill O P and Martinac B 2001 *Physiol. Rev.* **81** 685–740
[146] Sergunova V A, Kozlova E K, Myagkova E A and Chernysh A M 2015 *Gen. Reanimatol.* **11** 39–53